2018

Environmental Forensics Study of Crude Oil and Petroleum Product Spills in Coastal and Oilfield Settings: Combined Insights from Conventional GC-MS, Thermodesorption-GC-MS and Pyrolysis-GC-MS

Michael A. Kruge
krugem@mail.montclair.edu

José Luis Gallego
University of Oviedo

Azucena Lara-Gonzalo
University of Oviedo

Noemi Esquinas
University of Oviedo
Follow this and additional works at: https://digitalcommons.montclair.edu/earth-environ-studies-facpubs

Part of the Analytical Chemistry Commons, Environmental Chemistry Commons, Environmental Monitoring Commons, Geochemistry Commons, Oil, Gas, and Energy Commons, and the Organic Chemistry Commons

Environmental forensics study of crude oil and petroleum product spills in coastal and oilfield settings: Combined insights from conventional GC-MS, thermodesorption-GC-MS and pyrolysis-GC-MS.

Michael A. Kruge,

Earth & Environmental Studies Department, Montclair State University, Montclair (NJ) USA

José Luis R. Gallego, Azucena Lara-Gonzalo, and Noemi Esquinas

Environmental Technology, Biotechnology and Geochemistry Group, Campus de Mieres, University of Oviedo, Mieres (Asturias), Spain

Abstract

A representative set of five oil spill samples from four different regions displayed different product characteristics and different levels of weathering. Three of them were taken along shorelines affected by marine oil spill events, viz., Aboño and *Prestige* (Spain) and *Deepwater Horizon* (USA) and the other two were taken at inland oil spill sites (Angola and Kuwait). A multi-faceted environmental forensics approach revealed key molecular features. In addition to the conventional GC/MS analysis of saturated and aromatic fractions, the polar fractions also were analyzed, revealing a complex series of linear alkanones in those oil samples particularly enriched in aliphatics. Thermodesorption-GC-MS of the whole oils was also employed to further test its efficacy as a tool for the rapid fingerprinting of environmental contamination. The method was shown to accurately detect most of the essential features

1

recognized in the conventional GC-MS analysis of the saturated and aromatic fractions, although in some instances with less sensitivity and poorer resolution. Characteristics so recognized included the distributions of normal and isoprenoid alkanes, saturate and aromatic biomarkers, and polycyclic aromatic compounds such as alkylphenanthrenes and alkyldibenzothiophenes. Sequential pyrolysis of the post-thermodesorption residue and asphaltene pyrolysis yielded similar results, indicating that the residue consists primarily of asphaltenes. Thermodesorption and pyrolysis GC-MS also recognized substances likely to be associated with spill cleanup efforts that were not detected by conventional analysis.

Key Words

asphaltenes, petroleum biomarkers, polycyclic aromatic compounds, alkanones, Aboño (Spain) oil spill, Angola oil spill, Kuwait oil spill, Macondo oil spill, *Prestige* oil spill

1. Introduction

Techniques and applications for the chemical fingerprinting of spilled crude oil and petroleum products have developed increasing sophistication over recent decades (Stout and Wang, 2007). Besides conventional gas chromatography - mass spectrometry (GC-MS), advanced methods including compound specific stable isotope ratio mass spectrometry, two-dimensional GC, and Fourier transform ion cyclotron resonance mass spectrometry have proven their effectiveness (Gaines et al., 2007; Jeffrey, 2007; Chen et al., 2016). In studies of contaminated sites, when rapid analytical results with minimum sample preparation are desired, analytical pyrolysis-gas chromatography-mass spectrometry (Py-GC-

MS) has been employed (De Leeuw et al., 1986; Richnow et al., 1995; Kruge and Permanyer, 2004; Kruge et al., 2010; Kruge, 2015). Contaminants that escape detection by conventional analytical methods may be discovered (Lara-Gonzalo et al., 2015). At temperatures and durations commonly used for analytical pyrolysis (e.g., 610°C for 20 seconds) volatile and semi-volatile constituents may also be thermally desorbed and mixed with true pyrolysis products. To isolate the two types of materials, a separate thermodesorption step can be performed first, heating the sample at a lower temperature (e.g., 350°C). The thermodesorption method (TD-GC-MS) employs the same instrumentation as Py-GC-MS. Thus after the GC-MS analysis of the thermally-desorbed volatiles and semi-volatiles has finished, the remaining sample residue can be heated at the higher pyrolysis temperature and a second GC-MS analysis effected. The thermodesorption - sequential pyrolysis approach for the study of environmental contamination was pioneered decades ago (Whelan et al., 1980) and has been used fruitfully since (Faure and Landais, 2001; Kruge, 2015). Thermodesorption alone, without subsequent residue pyrolysis, has been recommended by regulators as an alternative analytical method (USEPA, 1996).

For this study, a diverse collection of five samples affected by spills at locations around the world has been assembled. These include the (1) Aboño fuel oil spill (oiled rocks on the Asturian coast, Spain), (2) *Prestige* heavy fuel spill (oiled rocks on the Galician coast, Spain), (3) *Deepwater Horizon* tarball (Alabama coast, USA), (4) Kuwait crude oil spill (oilfield soil, deliberate spill during the first Gulf war), and (5) an Angolan light crude oil spill (oilfield soil). In addition to conventional GC-MS analyses, thermodesorption-GC/MS and pyrolysis-GC-MS were employed. The data are interpreted in the context of the samples' diverse origins, emplacement, and weathering using a standard environmental forensics approach. In addition, insights from the thermodesorption and pyrolysis methods are presented, including an evaluation of their effectiveness as forensic screening tools.

2. Materials and Methods

2.1. Samples

A representative set of five samples obtained in four very different regions was selected in order to obtain a mixture of well-known spills and unknown cases, different product characteristics, and different levels of weathering. Three of them were taken in shorelines affected by marine oil spills and the other two were taken inland in areas where oil spill incidents had occurred.

The Kuwait sample is an oiled sandy soil partially preserved for years from weathering effects in very dry/anoxic conditions. It was taken in 2014 in one of the areas (Burgan field) affected by the huge spills that took place in the first Gulf War (Brown et al., 1998). A detailed description of oil geochemistry of Burgan field can be found in Kaufman et al. (2000). The sample is from a "dry oil lake" in which the polluted sand (taken at 40 cm depth, having 20,000 ppm total petroleum hydrocarbons; TPH) was encrusted with a surficial layer of weathered heavy oil that preserved the product permeating the sand below from rapid degradation. The soil is sealed by a tar mat (Balba et al., 1998), forming a layer about 1 cm thick that was peeled off to reveal the underlying polluted sand that was sampled. The soil sampled revealed an alkaline pH, high salinity, sandy texture (less than 10% of silt and clay), and very low concentrations of nitrogen, phosphorus and natural organic matter. Information on the composition of this particular fresh oil was not available, but reported mean values for three topped fresh Burgan field oils are 37.7% saturated hydrocarbons, 46.0% aromatics, 8.1% polar compounds, and 8.3% asphaltenes, with 2.93% sulfur in the whole oil (Abdullah and Connan, 2002).

The sample from Angola was taken in 2012 in a sandy soil affected by oil spills (TPH: 11,000 ppm) as a result of oil exploration and production activity at a confidential location. The soil sampled shown a neutral pH, low conductivity, sandy texture (less than 10% of silt and clay), and low

concentrations of nitrogen, phosphorus and natural organic matter. Compositional data on the fresh crude oil were not obtainable.

At the end of June 2012, the Cantabrian shoreline of Asturias (Spain) was affected by a heavy fuel oil spill (around 20 tons) from an industrial facility close to the coast. The Aboño sample was taken in a study site with a relatively homogenous 500 m stretch of pristine rocky shore affected by the fuel immediately after the spill. In order to obtain representative data, composite samples comprised ten increments of 4 cm^2 of fuel geometrically distributed at sampling stations, corresponding to rocks from the upper intertidal zone (Gallego et al., 2013). The Aboño spill was originated by a heavy fuel oil ($\delta 15°C = 0.991$ kg/L; sulfur=2.25%) composed when fresh of 24.3% saturates, 44.2% aromatics, 11.5% polars, and 20.0% asphaltenes.

Like the Aboño, the *Prestige* sample is a rock scraping. It was obtained in 2010, more than 7 years after the *Prestige* fuel oil spill (Alzaga et al., 2004), at the beach site called Moreira, located on the Atlantic coast of Galicia (northwestern Spain), 80 km from La Coruña. Significant weathering and specifically (bio)degradation was expected given that this area was subjected to bioremediation with oleophilic fertilizers between 2003 and 2005 (Gallego et al., 2006). The spilled cargo of the *Prestige* tanker was a heavy residual fuel oil ($\delta 15°C = 0.993$ kg/L; sulfur $= 2.6\%$; nitrogen $= 0.69\%$) that was composed of 26.8% saturates, 39.1% aromatics, 17.3% polars, and 16.8% asphaltenes (Díez et al., 2005; Gallego et al., 2007).

The Macondo sample is a tarball recovered along the Alabama shoreline approximatly six weeks following the explosion of the *Deepwater Horizon* oil rig on April 20, 2010. That tragic event led to a release of more than 70,000 tons of petroleum hydrocarbons from the Macondo well (Atlas and Hazen, 2011). The Macondo oil has been intensively studied in recent years, and therefore its composition (chemical fingerprint, biomarkers, weathering evolution etc.) is well known (Aeppli et al., 2012; Aeppli

et al., 2014; White et al., 2016). The fresh Macondo oil was a light crude oil ($\delta 15°C$ = 0.820 kg/L; sulfur = 0.4%; nitrogen = 0.38%) with 74% saturates, 16% aromatics, and 10% resins and asphaltenes (Reddy et al., 2012).

2.2. Experimental Methods

Figure 1 presents an overview of the experimental procedures, the details of which are given below.

<INSERT FIGURE 1 HERE>

Figure 1. Analytical scheme used in this study.

2.2.1. Extraction and LC Fractionation

The sandy samples (Kuwait and Angola) were extracted with dichloromethane:methanol (3:1, v/v) in a Soxtherm system (Gerhardt). The extract was concentrated by rotary evaporation. The shoreline samples (rock scrapings from *Prestige* and Aboño spills, and sand from DWH spill) were extracted as follows: 1-g representative subsamples were extracted with dichloromethane in an ultrasonic bath for 15 min; the extracts were then carefully filtered (Whatman 42 filter) to eliminate impurities such as sand, clay particles, algae.

Aliquots of the extracts (both soil and shoreline samples) were fractionated and gravimetrically quantified by liquid chromatography (LC) into saturated and aromatic hydrocarbon, polar compound, and asphaltene fractions. In brief, LC was carried out in two steps: in the first one, maltenes and

Figure 1
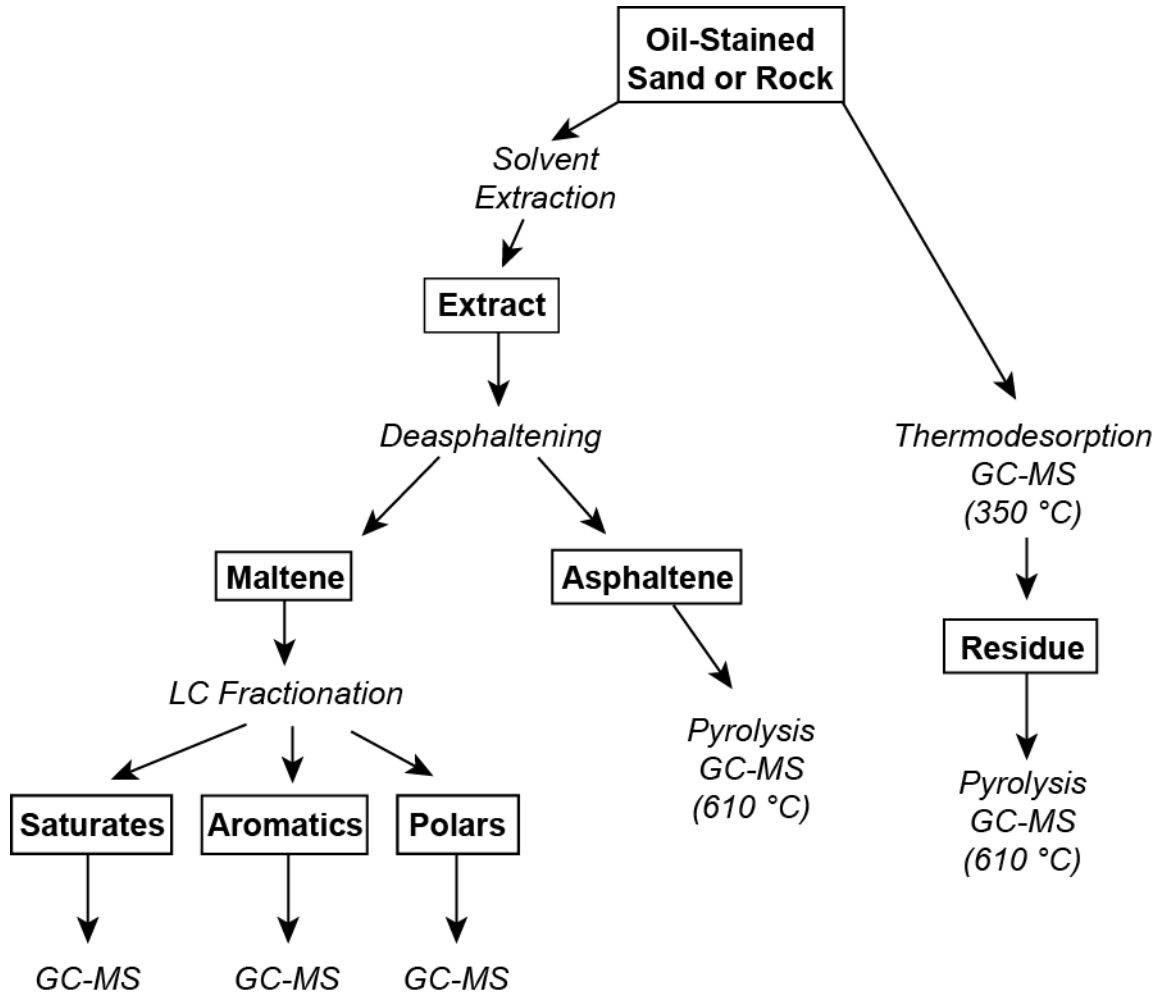
asphaltenes were separated by filtering through 0.45 μm filters using hexane and dichloromethane, respectively; then, in the second step, maltenes were fractionated into saturated, aromatic, and polar fractions by LC in columns filled with silica gel and alumina. The saturated fraction was eluted with hexane, the aromatics with a mix of dichloromethane:hexane (4:1, v/v) and finally, the polar fraction with dichloromethane:methanol (1:1, v/v).

2.2.2. Conventional GC-MS

The analyses of the saturate, aromatic, and polar fractions were carried out by gas chromatography-mass spectrometry (GC-MS). The injection of the extracts was performed on a GCMS-QP2010 Plus from Shimadzu. A capillary column DB-5ms (5% phenyl 95% dimethylpolysiloxane; 60 m × 0.25 mm i.d. × 0.25 μm film) from Agilent Technologies was used with helium as carried gas at 1 mL min^{-1}. The initial oven temperature was 40ºC (held for 5 min) and ramped at 5ºC min^{-1} up to 300ºC and held for 20 min. The mass spectrometer was operated in electron ionization mode (EI) at 70 eV. It was calibrated daily by autotuning with perfluorotributylamine (PFTBA) and the chromatograms were acquired in full-scan mode (mass range acquisition was performed from 45 to 500 m/z). For quality control, solvent blanks were periodically injected.

2.2.3. Thermodesorption-GC-MS and Pyrolysis-GC-MS

Aboño, Angola, Kuwait oil-stained rock and sands. Oil scraped from the stained rock (Aboño, < 0.1 mg) and oil-stained sand (Angola, Kuwait, ca. 5-6 mg) were analyzed by thermodesorption-gas chromatography-mass spectrometry (TD-GC-MS) using a CDS 5150 Pyroprobe coupled to a Thermo

Finnigan Focus DSQ GC/MS equipped with an Agilent DB-1MS column (30 m × 0.25 mm i.d. × 0.25 µm film thickness). The GC oven temperature was programmed from 50°C to 300°C (at 5°C min^{-1}), with an initial hold of 5 minutes at 50°C and a final hold of 15 minutes at 300°C. The MS was operated in full scan mode (50-500 Da, 1.08 scans sec^{-1}). After the thermodesorption run ended, the sample (which had remained untouched in the Pyroprobe) was heated at 610°C for 20 sec, pyrolyzing the post-thermodesorption residue ("sequential pyrolysis"). Pyrolysis products were analyzed by GC-MS (Py-GC-MS) using the conditions employed for the thermodesorption products.

Prestige oil-stained rock. Rock scraping of the *Prestige* spilled oil (0.22 mg) was analyzed with a PY-2020iD double-shot pyrolyzer (Frontier Lab) coupled to a Shimadzu GCMS-QP2010 equipped with a DB-5ms column (30 m × 0.25 mm i.d. × 0.25 µm film). The GC oven temperature was programmed from 50°C to 300°C (at 5°C min-1), with an initial hold of 5 minutes at 50°C and a final hold of 30 minutes at 300°C. Thermodesorption was effected for 20 seconds at 350°C. Upon completion of the GC run, the residue was pyrolyzed for 20 seconds at 610°C and a second GC run completed. The MS was operated in full scan mode from 50 to 500 Da.

Asphaltenes. Py-GC-MS (610°C, 20 sec) was performed directly on the asphaltene fractions (<0.1 mg), without the thermodesorption step. Py-GC-MS instrumentation and conditions were the same as those used for the Aboño, Angola, and Kuwait oil-stained rock and sands.

Macondo tarball. Unlike the others, this sample (<0.1 mg) was analyzed in a "single shot" run at 610°C for a rapid, combined thermodesorption-pyrolysis experiment. For this, a CDS 2000 Pyroprobe was coupled to a Thermo Finnigan Focus DSQ GC/MS equipped with a J&W DB-1MS column (15 m × 0.25 mm i.d. × 0.25 µm film thickness). The GC oven temperature was programmed from 50°C to 300°C (at 5°C min-1), with an initial hold of 5 minutes at 50°C and a final hold of 5 minutes at 300°C.

Pyrolysis was performed for 20 seconds at 610°C. The MS was operated in full scan mode (50-500 Da, 1.08 scans sec-1).

3. Results and Discussion

3.1. Overview of General Characteristics

The five samples discussed in this chapter represent a variety of spill types (crude oils and petroleum products) from marine and terrestrial settings. They are genetically unrelated and represent wide compositional variety. The Kuwait oil was a normal, but sulfur-rich crude spilled in the oil field at the end of the first Gulf War, degraded during years of residence at the surface. The Aboño sample was a fuel oil product spilled at sea, subsequently contaminating shore areas. The *Prestige* sample had a similar history, but originated as a heavier fuel oil fraction. The Angola sample is a light crude oil, spilled in the oil field. The Macondo sample was spilled at sea and subsequently collected after it made landfall. In their present state, the Kuwait and Aboño samples are considered to be heavy degraded oils, following the classification of Tissot and Welte (1984), with the Aboño sample richer in aromatic hydrocarbons (Figure 2; Table 1). The *Prestige* sample exhibits a more extreme level of degradation, composed primarily of polar compounds and, especially, asphaltenes. In contrast, the Angola sample contains mostly saturated hydrocarbons. Saturated hydrocarbons comprise nearly half of the Macondo sample, which is also notably poor in aromatics. In their present degraded state, the Angola and Macondo samples are low in sulfur, while the other three are sulfur-rich, in particular the Kuwait, having 6.3 % sulfur (Table 1).
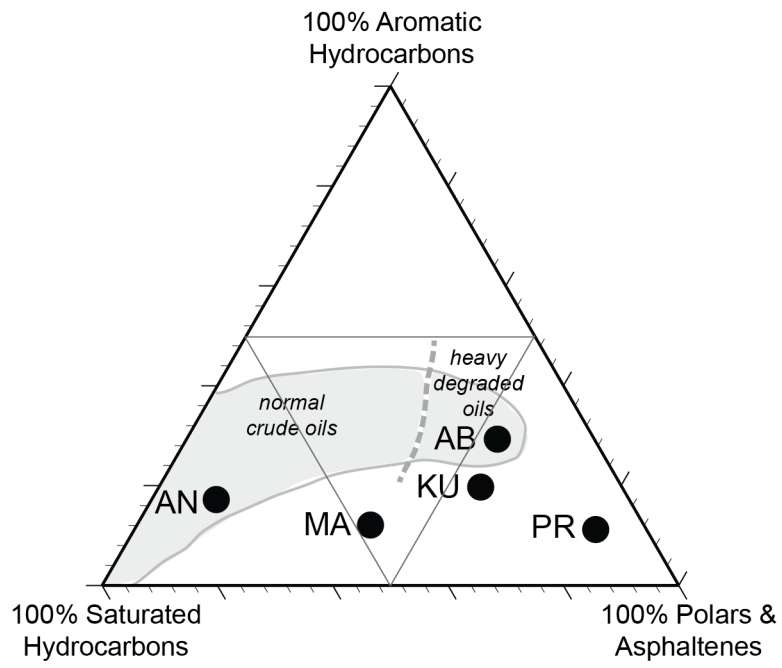
<INSERT FIGURE 2 HERE>

Figure 2

Figure 2. Ternary diagram showing the bulk composition of the five degraded oil samples as reported in Table 1. AB: Aboño, AN: Angola, KU: Kuwait, MA: Macondo, PR: *Prestige*. The "normal" and "heavy degraded" zonations follow Tissot and Welte (1984).

<INSERT TABLE 1 HERE>

Table 1. Bulk composition of the degraded oils, as received.

For an overview of their principal molecular characteristics, total ion chromatograms (TIC) of the saturated and aromatic hydrocarbon fractions derived from the solvent extract are presented along with traces from thermodesorption of the whole sample at 350°C, the subsequent pyrolysis of the same sample aliquot at 610°C, and the pyrolysis of the asphaltene fraction, also at 610°C. Chromatographic conditions and instrumentation varied depending on sample type, as discussed in detail above. Details of specific compounds (including normal alkanes, biological marker compounds, and aromatic hydrocarbons) are presented subsequently in section 3.2.

3.1.1. Kuwait Oil Spill

The total ion current trace of the Kuwait oil's saturated hydrocarbon fraction displays prominent normal alkanes from C_{16} to at least C_{30}, phytane, pristane, and C_{29}-C_{35} hopanes (Figure 3A). Their peaks crown a broad unresolved complex mixture (UCM) hump in the n-C_{15}-C_{40} retention time range.

Table 1.

Sample	Saturates (%)	Aromatics (%)	Polars (%)	Asphaltenes (%)	Sulfur (%)
Aboño	16.8	29.3	26.2	27.7	3.2
Angola	71.6	17.2	7.9	3.3	0.9
Kuwait	24.5	19.7	35.6	20.2	6.3
Macondo	47.4	12.1	22.1	18.4	0.9
Prestige	8.8	11.2	12.5	67.5	3.2

The aromatic fraction exhibits a UCM hump spanning the same retention times (Figure 3B). Clearly evident aromatic compounds include a series of C_1 to C_4-alkylated dibenzothiophenes, consistent with this oil's high sulfur content (Table 1). Also noteworthy are aromatic biomarkers, including 8,14-secohopanoids and benzohopanes.

<INSERT FIGURE 3 HERE>

Figure 3. Total ion current chromatograms for the Kuwait oil. A) saturated hydrocarbon fraction, B) aromatic fraction, C) thermodesorption products, D) products of sequential pyrolysis of the post-thermodesorption residue, and E) asphaltene pyrolysis products. See Table 2 for peak identification.

<INSERT TABLE 2 HERE>

Table 2. Symbols used for peak identification in Figures 3 to 12, 14 and 15.

The composition of thermodesorption products is expected to resemble that of the full solvent extract prior to fractionation. This is generally the case with the Kuwait sample, for which the thermodesorption TIC shows a pronounced UCM hump in the n-C_{15}-C_{40} range, with hopanes, minor n-alkanes, phytane, and alkyldibenzothiophenes clearly in evidence (Figure 3C). These compounds were all detected in either the saturated or aromatic fractions, but occur in different proportions in the thermally desorbed components. The thermodesorption results provide a convenient means for assessing the extent of biodegradation, providing in effect a "whole oil" chromatogram that also shows some of the volatiles lost when using the solvent extraction method. From examination of Figure 3C it is evident that the oil is heavily biodegraded, i.e., having a value of 3-4 on the 10 point biodegradation
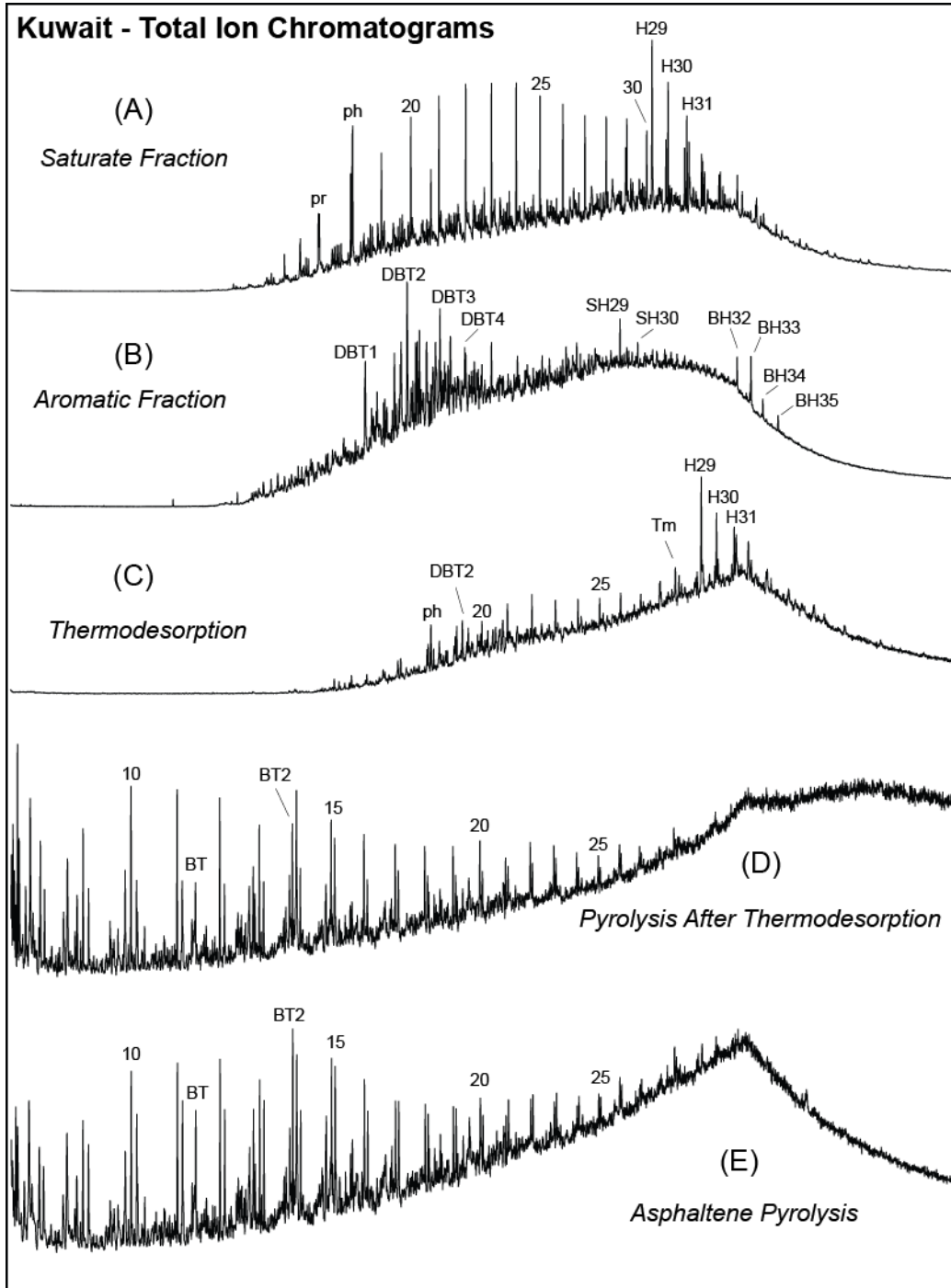
Figure 3

Kuwait - Total Ion Chromatograms

(A) Saturate Fraction

(B) Aromatic Fraction

(C) Thermodesorption

(D) Pyrolysis After Thermodesorption

(E) Asphaltene Pyrolysis

Table 2.

Saturated Hydrocarbons

numerals	normal alkanes (*n*-alk-1-ene/*n*-alkane doublets for pyrolyzates)
pr	pristane
ph	phytane
Hx	hopanes ("x" indicates the carbon number, C_{29}-C_{35})
Ts	$18\alpha(H)$-22,29,30-trisnorhopane
Tm	$17\alpha(H)$-22,29,30-trisnorhopane
TRx	tricyclic terpanes ("x" indicates the carbon number)
Sx	regular steranes ("x" indicates the carbon number)
Dx	diasteranes ("x" indicates the carbon number)
#	*n*-alkylcyclohexanes

Aromatic Compounds

For alkyl-substituted aromatic compounds, "x" indicates the degree of substitution.
1: methyl, 2: dimethyl or ethyl, etc.

Bx	alkylbenzene isomers
ST	styrene
*	*o*-alkyltoluenes
N	naphthalene
Nx	alkylnaphthalene isomers
PHN	phenenanthrene
PHNx	alkylphenanthrene isomers
ANT	anthracene
PYRx	alkylpyrene isomers
CHR	chrysene
CHRx	alkylchrysene isomers
BAN	benzo[*a*]anthracene
BANx	alkylbenzo[*a*]anthracene isomers
BT	benzothiophene
BTx	alkylbenzothiophene isomers
DBT	dibenzothiophene
DBTx	alkyldibenzothiophene isomers
BNT	benzonaphthothiophene
SHx	8,14-secohopanoids ("x" indicates the carbon number)
BHx	benzohopanes ("x" indicates the carbon number)
TASx	triaromatic steroids ("x" indicates the carbon number)

Other Compounds

Ax	*n*-alkanoic acids ("x" indicates the carbon number)
IBx	isobutylene oligomers ("x" indicates the carbon number)

scale of Peters et al. (2005), since relatively minor amounts of *n*-alkanes are still present. The residue

remaining after thermodesorption was pyrolyzed, yielding a mixture of lower molecular weight

compounds contrasting strongly with the thermally desorbed mixture (Figures 3C, 3D). Most notably,

the trace displays a series of C_7-C_{27} *n*-alk-1-ene/*n*-alkane doublets characteristic of the pyrolysis

products of aliphatic-rich material (e.g., Kruge, 2015). Benzothiophenes are also present, indicative of

the sulfurous nature of the sample. While isoprenoids and hopanes are important thermodesorption

products, they are not detectable in the pyrolyzate. The pyrolyzate of the extract's asphaltene fraction

(Figure 3E) closely resembles that of the residue (Figure 3D), with prominent n-alk-1-ene/n-alkane pairs

and benzothiophenes. This suggests that much of the material remaining after thermodesorption is

asphaltene.

3.1.2. Aboño Fuel Oil Spill

The saturated hydrocarbon fraction of the degraded Aboño fuel oil notably contains long-chain

n-alkanes (C_{23}-C_{33}), hopanes, and isoprenoids. Its TIC trace displays a prominent UCM hump in the *n*-

C_{14} to C_{40} retention time range (Figure 4A). Its aromatic fraction is characterized by a UCM hump over

the same retention times, with a complex distribution of polycyclic aromatic hydrocarbons (PAHs),

particularly alkylphenanthrenes and alkylchrysenes (Figure 4B). As with the Kuwait sample, the

thermodesorption products combine features detected in the saturated and aromatic fractions, in this case,

prominent UCM hump, alkylated PAHs, and lesser amounts of long-chain *n*-alkanes (Figure 4C). The

relatively abundant PAHs evident in the aromatic fraction and thermally desorbed material are

consistent with the sample's elevated aromatic content (Table 1). This heavily biodegraded sample fits

the description corresponding to levels 3-4 on the Peters et al. (2005) biodegradation scale. The

pyrolyzates of both the post-thermodesorption residue and the asphaltenes show a predominance of

aliphatic hydrocarbons (short- to mid-chain n-alkanes and alkenes) with secondary amounts of aromatic

compounds such as methylnaphthalene and benzothiophene (Figures 4D, 4E).
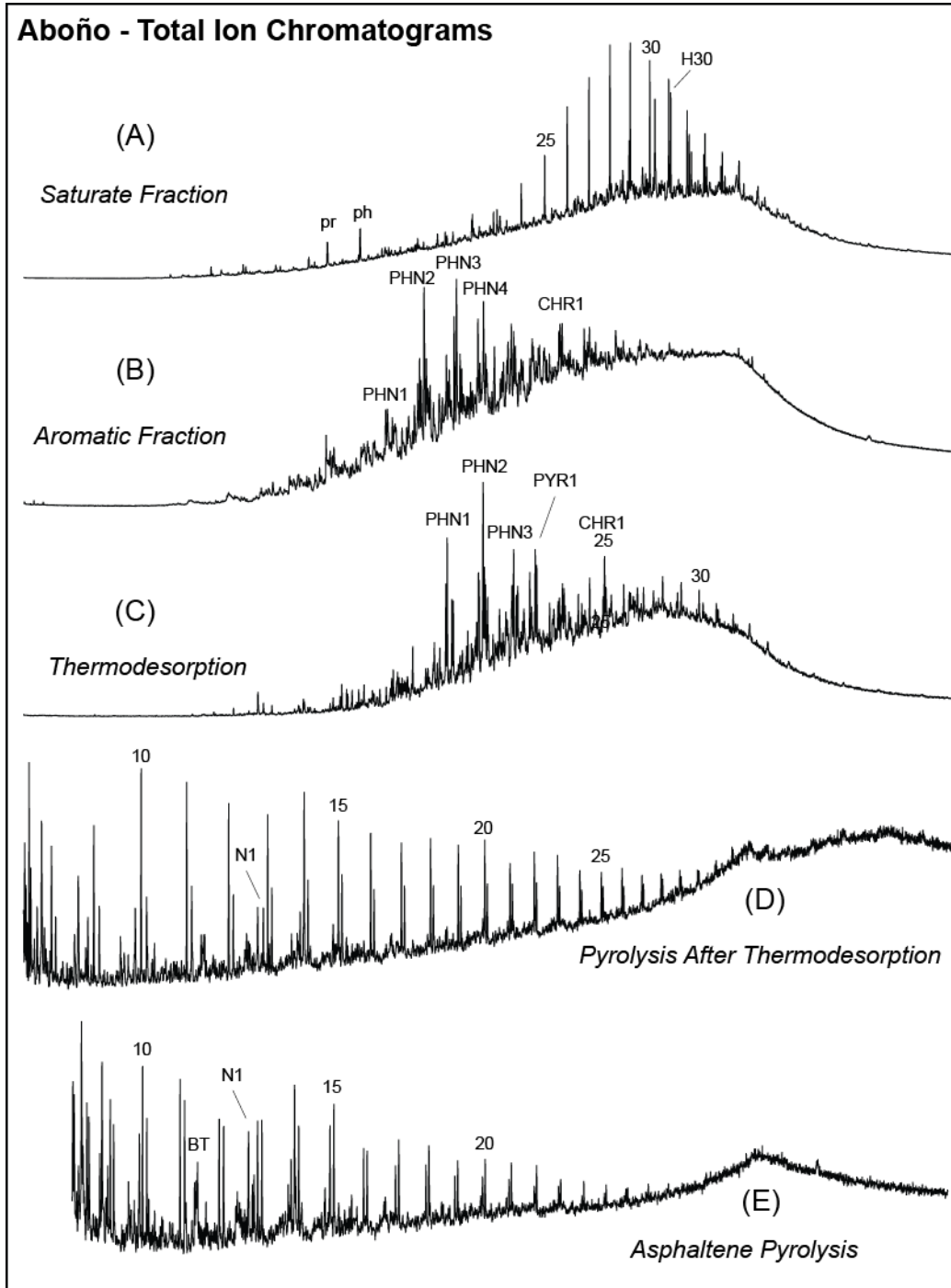

<INSERT FIGURE 4 HERE>

Figure 4. Total ion current chromatograms for the Aboño fuel oil. A) saturated hydrocarbon fraction, B)

aromatic fraction, C) thermodesorption products, D) products of sequential pyrolysis of the post-

thermodesorption residue, and E) asphaltene pyrolysis products. See Table 2 for peak identification.

3.1.3. Prestige Fuel Oil Spill

The saturated hydrocarbons isolated from the degraded *Prestige* heavy fuel oil contain long-

chain n-alkanes ranging from C_{24} to C_{42} and beyond, along with hopanes. The UCM hump also reflects

the predominance of heavier hydrocarbons, covering the n-C_{19} to n-C_{42} retention time range, with its

maximum coeluting with n-C_{36} (Figure 5A). The TIC trace of the aromatics exhibits a prominent UCM

hump with a plateau in the n-C_{29} to C_{36} retention time range (Figure 5B). PAHs (phenanthrenes,

pyrenes, chrysenes) and aromatic biomarkers including 8,14-secohopanoids, benzohopanes, and

triaromatic steroids are also in evidence. Upon thermodesorption, the sample yielded long-chain n-

alkanes and hopanes consistent with those seen in the saturated fraction (Figures 5A, 5C), as well as a

prominent UCM hump having a maximum coincident with n-C_{30}. The C_{16} and C_{18} fatty acids are likely

from residue of an oleophilic fertilizer sprayed at the spill site to favor biodegradation (Gallego et al.,

2006), as the material to be thermodesorbed was scraped directly from a tar-stained rock sample with no

Figure 4

Aboño - Total Ion Chromatograms

(A) Saturate Fraction

(B) Aromatic Fraction

(C) Thermodesorption

(D) Pyrolysis After Thermodesorption

(E) Asphaltene Pyrolysis

preparative steps. This sample exhibits severe biodegradation or 4-6 on the Peters et al. (2005) scale, although for reasons of bioavailability it has long chain n-alkanes still evident as major components. The residue after thermodesorption is predominantly aliphatic (Figure 5D), as is the asphaltene pyrolyzate (Figure 5E), although the latter has relatively more aromatic hydrocarbons, particularly alkylbenzenes and alkylnaphthalenes, and a pronounced UCM hump.
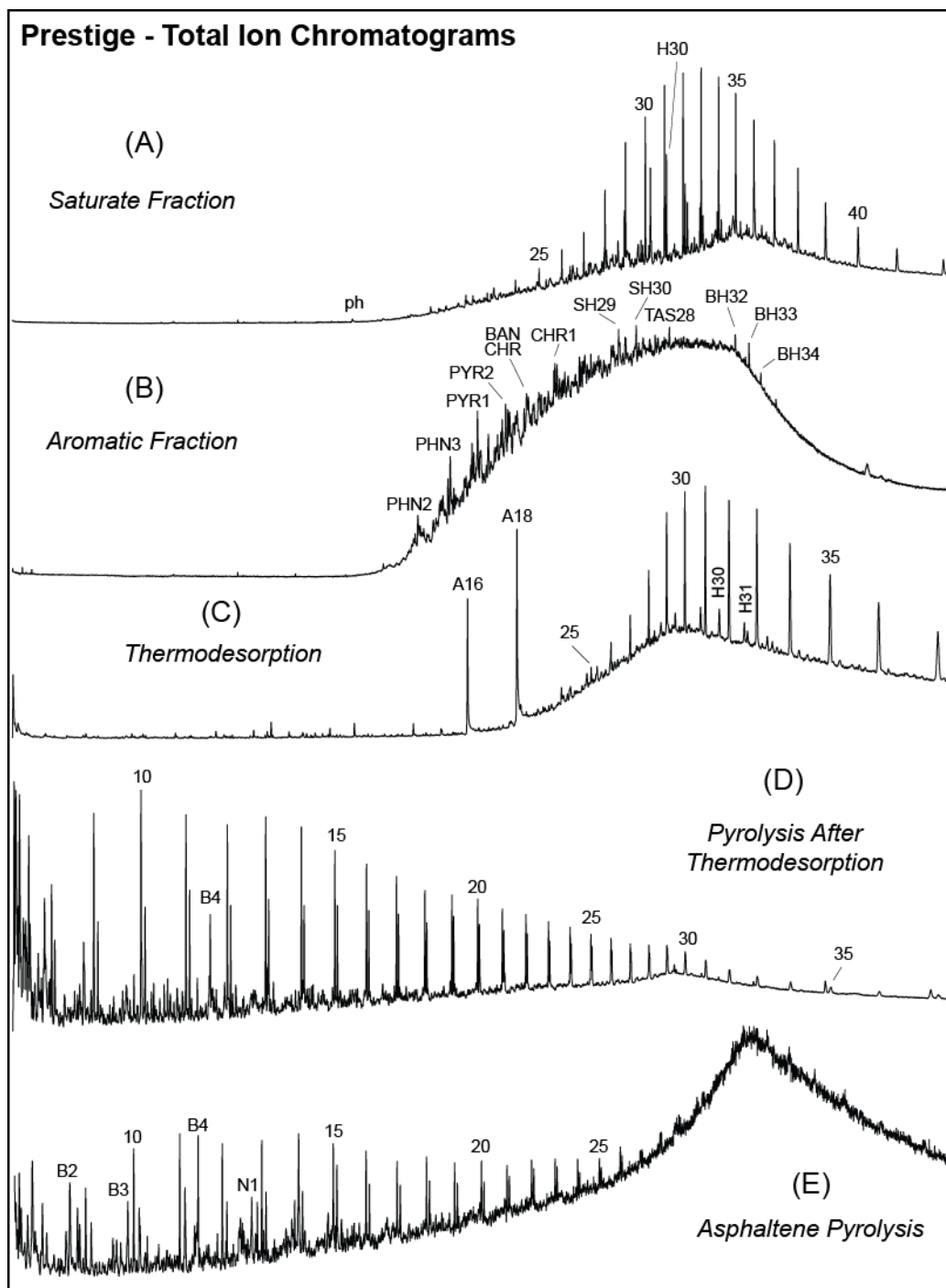
<INSERT FIGURE 5 HERE>

Figure 5. Total ion current chromatograms for the Prestige fuel oil. A) saturated hydrocarbon fraction, B) aromatic fraction, C) thermodesorption products, D) products of sequential pyrolysis of the post-thermodesorption residue, and E) asphaltene pyrolysis products. See Table 2 for peak identification.

3.1.4. Angola Oil Spill

The light Angola petroleum is distinguished from the other samples in this study by its very high saturated hydrocarbon content (71.6 %, Table 1). Its TIC chromatograms reflect its distinctiveness. The saturated fraction exhibits a series of n-alkanes from C_{13} to C_{27}, with a maximum at C_{20} along with lesser amounts of isoprenoids and hopanes (Figure 6A). Its UCM hump attains its maximum coincident with n-C_{28} and extends to the n-C_{37} retention time. The aromatic TIC trace is dominated by a similar UCM hump (Figure 6B). With PAHs relatively less abundant, this fraction is instead notable for a series of C_{16}-C_{29} o-alkyltoluenes and other long-chain alkylbenzenes, indicating that even its aromatic hydrocarbons have an "aliphatic" character. The thermally-desorbed components closely resemble those of the dominant saturated fraction, having a similar distribution of normal alkanes, isoprenoids and

Figure 5

Prestige - Total Ion Chromatograms

(A) Saturate Fraction

(B) Aromatic Fraction

(C) Thermodesorption

(D) Pyrolysis After Thermodesorption

(E) Asphaltene Pyrolysis

hopanes (Figure 6C). There is also a relatively narrow UCM hump maximizing near n-C_{30}. With n-alkanes still present, this sample can be considered to be lightly to moderately biodegraded, that is, at level 1-2 on the Peters et al. (2005) scale. Very little residue remained after thermodesorption. The most prominent peaks evident on its TIC chromatogram are interpreted to correspond to isobutylene oligomers ((C_4H_8)$_n$) from the pyrolysis of polyisobutylene. This polymer is employed in oil spill cleanup (Vollhardt and Schore, 2002) and its detection here is forensic evidence suggesting that it may have been used for remediation at the Angolan site. These compounds were not detected in any of the extract fractions and therefore must only be present as pyrolysis products. They were not found in the asphaltene pyrolyzate either (Figure 6E). The only prominent peak on its TIC trace is due to styrene, suggesting polystyrene contamination at the collection site or during handling. In any case, asphaltenes constitute only a very minor portion of this oil (3.3 %, Table 1).

<INSERT FIGURE 6 HERE>

Figure 6. Total ion current chromatograms for the Angola oil. A) saturated hydrocarbon fraction, B) aromatic fraction, C) thermodesorption products, D) products of sequential pyrolysis of the post-thermodesorption residue, and E) asphaltene pyrolysis products. See Table 2 for peak identification.

3.1.5. Macondo Oil Spill

The Macondo tarball sample was collected about six weeks after the start of the spill event, shortly after the material reached the Alabama shore. It is relatively fresh, with abundant n-alkanes (C_{16}-C_{42}, maximum at C_{20}) in its saturated fraction, along with subordinate isoprenoids and n-

Figure 6

Angola - Total Ion Chromatograms

(A) *Saturate Fraction*

(B) *Aromatic Fraction*

(C) *Thermodesorption*

(D) *Pyrolysis After Thermodesorption*

(E) *Asphaltene Pyrolysis*
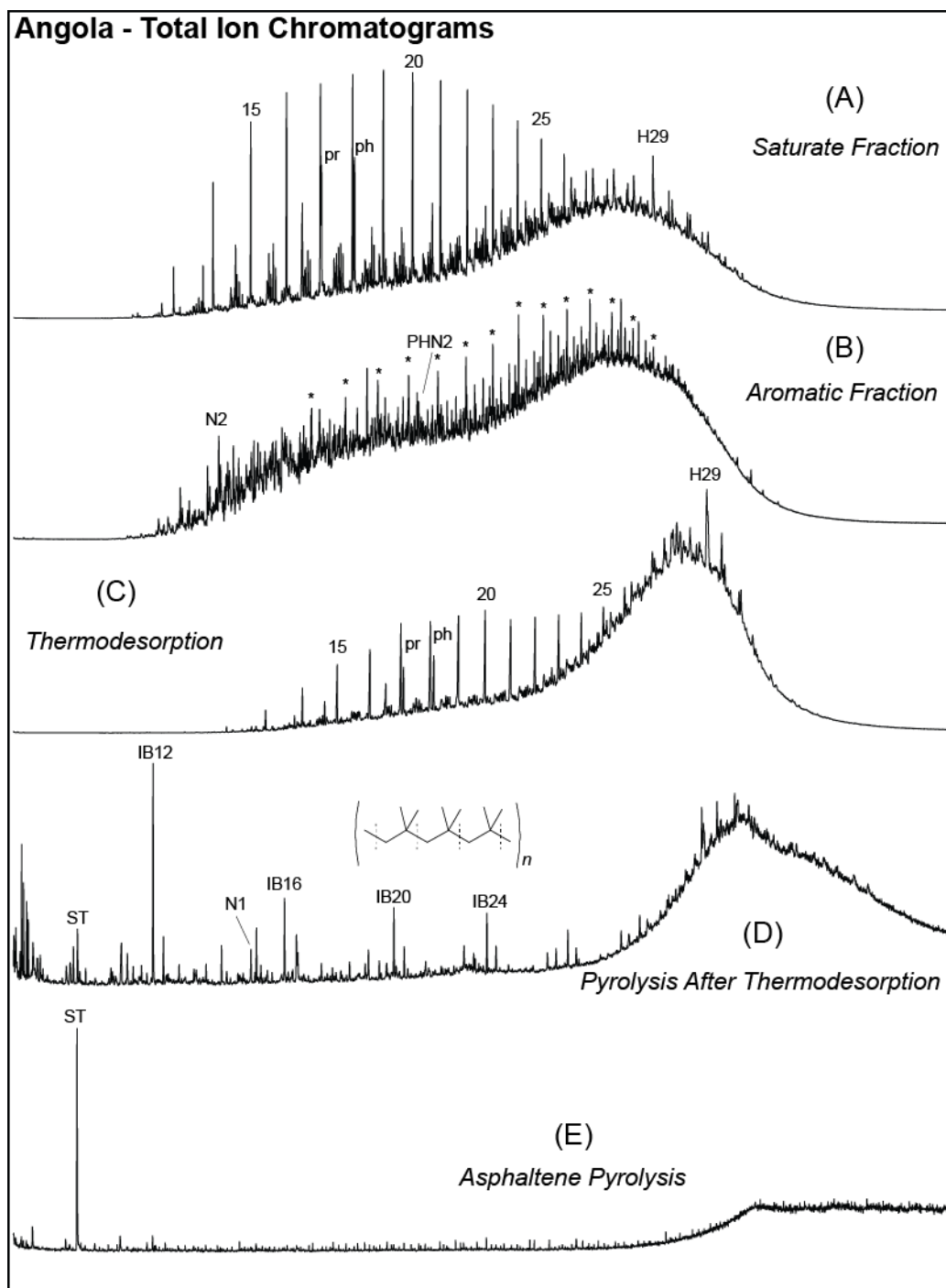
alkylcyclohexanes (Figure 7A). The UCM hump is more apparent in the aromatic fraction, along with phenanthrenes and benzo[*a*]anthracenes (Figure 7B). As with the Angola sample, there are also long-chain alkylbenzenes present, most notably, the *o*-alkyltoluene series from C_{17} to C_{30}. For this sample, a "single shot" combined thermodesorption and pyrolysis experiment was employed, heating the sample only once at 610°C and using a short (15 m) GC column to reduce analysis time and favor the elution of the heavier compounds. The results are essentially similar to those in the saturate fraction (Figures 7A, 7C), with a predominance of C_{16}-C_{33} *n*-alkanes, pristane, phytane, and C_{18}-C_{23} *n*-alkylcyclohexanes. This is to be expected since saturated hydrocarbons comprise nearly half of the sample (Table 1). Notably absent from Figure 7C are the normal alkane/alkene doublets characteristic of the pyrolysis of aliphatic-rich material and seen in the pyrolyzates of the other samples (Figures 3D, 4D, 5D). It is evident therefore that nearly all of the sample was thermally desorbed and thereby avoided pyrolysis. It will be treated as the equivalent of a thermodesorption product in the discussions below. In contrast with the other samples in this study, the Macondo tarball is only moderately biodegraded, having approximately a value of 2 on the 10 point scale of Peters et al. (2005).

<INSERT FIGURE 7 HERE>

Figure 7. Total ion current chromatograms for the Macondo oil. A) saturated hydrocarbon fraction, B) aromatic fraction, C) combined thermodesorption and pyrolysis products produced in a single shot run at 610 °C. See Table 2 for peak identification.

3.2. Principal Compound Groups

16

Figure 7

Macondo - Total Ion Chromatograms

(A) Saturate Fraction

(B) Aromatic Fraction

(C) Combined Thermodesorption & Pyrolysis
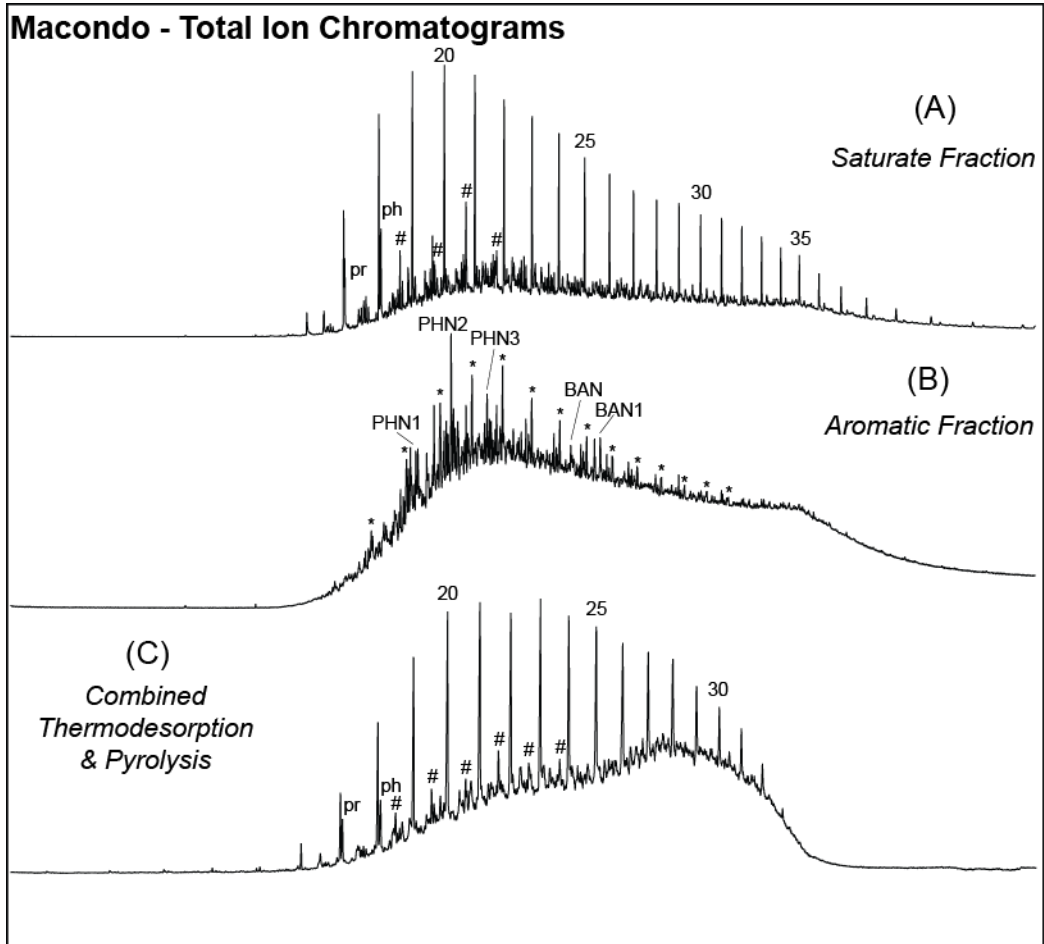
3.2.1. Aliphatic Hydrocarbons

For a clearer picture of the normal and isoprenoid alkane distributions in the sample set, *m/z* 71 mass chromatograms are plotted in Figure 8. From the top to the bottom of the diagram, the samples are arranged in order of decreasing saturated hydrocarbon content (Table 1). Coincidently, there is a corresponding shift from predominantly shorter to longer chains proceeding from the Angola sample (Figures 8A, 8B) to the *Prestige* (Figures 8I, 8J). The traces from the saturate fractions are arrayed on the left side of Figure 8, with their thermodesorption counterparts on the right. While similarities were noted when comparing the TIC chromatograms of the Angola saturates and thermodesorption products (Section 3.1.4; Figures 6A, 6C), the *m/z* 71 traces show a much stronger correspondence in the distribution of alkanes (Figures 8A, 8B), all the more so when taking into account the differences in chromatographic conditions employed (Section 2.2). On both chromatograms, one observes a predominance of C_{14} to C_{25} *n*-alkanes, with a maximum around C_{18} or C_{19}, and a pristane/phytane ratio close to unity. For the Macondo sample, the longer chain *n*-alkanes ($> C_{33}$) are more effectively detected by the injection technique (Figure 8C) than by thermodesorption (Figure 8D). Otherwise the alkane distributions correspond closely, beginning with *n*-C_{16} and maximizing at C_{20}. The Kuwait chromatograms display the same range of *n*-alkanes (C_{16}-C_{36}, maximum at C_{22}), but there are variations in the distributions (Figures 8E, 8F). Both techniques revealed a low pristane/phytane ratio, although phytane appears relatively more abundant overall in the thermodesorption products. The mid-length alkanes appear more abundant in the thermally desorbed components of the Aboño oil than in its saturate fraction, with a maximum at *n*-C_{26} rather than C_{29} (Figures 8G, 8H). With both methods, however, the *n*-alkane range is shown to extend to about C_{36} and phytane is marginally more abundant than pristane. With the heavy *Prestige* fuel oil, both techniques revealed a preponderance of long-chain

17

n-alkanes, with the maximum at C_{30} or C_{31} and very little eluting prior to C_{24} (Figures 8I, 8J). The thermodesorption results indicate the presence of *n*-alkanes up to C_{42} (not shown in Figure 8J). Fatty acids noted on the thermodesorption TIC trace (Figure 5C) are also evident here. Pristane/phytane ratios in the thermodesorption products are close to those in the saturate fraction (Table 3).

<INSERT FIGURE 8 HERE>

Figure 8. Mass chromatograms (*m/z* 71) showing the distribution of normal and isoprenoid alkanes in the saturate fractions (A, C, E, G, I) and corresponding thermodesorption products (B, D, F, H, J) of the five oils. See Table 2 for peak identifications.

<INSERT TABLE 3 HERE>

Table 3. Diagnostic molecular ratios for the saturated (SAT) and aromatic (ARO) fractions and the thermodesorption products (TD), computed using the indicated ions for the five oil samples. mPHN: methylphenanthrene, mDBT: methyldibenzothiophene, Pr: pristane, Ph: phytane, H29: $17\alpha(H),21\beta(H)$-30-norhopane, H30: $17\alpha(H),21\beta(H)$-hopane. * compound concentrations too low; ** combined thermodesorption/pyrolysis "single-shot" data employed.

3.2.2. Hopanes and Steranes

The *m/z* 191 mass chromatograms displaying hopane distributions are arrayed in Figure 9 using the same sequence employed in Figure 8, with the sample most enriched in saturated hydrocarbons on
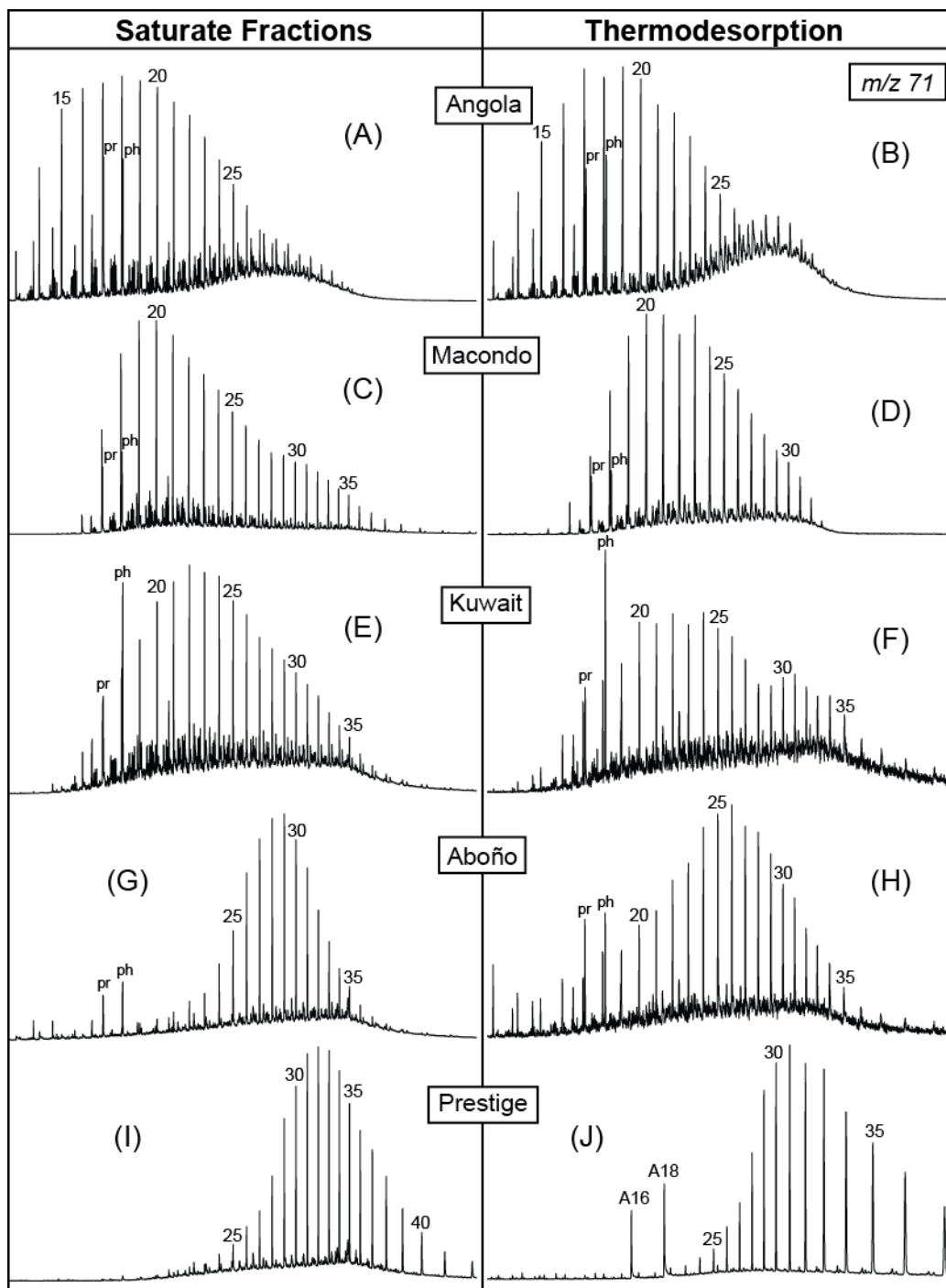
Figure 8

Table 3.

m/z	192	198	71	191
Diagnostic ratio	2-mPHN/1-mPHN	4-mDBT/1-mDBT	Pr/Ph	H29/H30
Aboño TD	1.83	2.50	0.92	0.88
Aboño ARO/SAT	1.35	2.88	0.84	0.75
Angola TD	1.28	3.09	0.93	1.47
Angola ARO/SAT	1.21	3.29	0.87	1.24
Kuwait TD	0.83	1.73	0.48	1.20
Kuwait ARO/SAT	0.75	1.83	0.43	1.26
Macondo TD**	1.51	3.02	0.84	0.38
Macondo ARO/SAT	1.23	2.95	0.90	0.43
Prestige TD	1.5	(*)	(*)	0.86
Prestige ARO/SAT	(*)	(*)	0.28	0.79

top of the diagram and the thermodesorption results placed to the right of the corresponding saturate fraction data. The Angola hopanes show a predominance of the C_{29} 17α(H),21β(H)-30-norhopane over the C_{30} 17α(H),21β(H)-hopane (peaks H29 and H30 respectively in Figures 9A and 9B, and Table 3) and a gradual decrease in relative abundance out to C_{35}. The C_{27} 18α(H)-22,29,30-trisnorhopane is nearly as abundant as the 17α(H)-22,29,30-trisnorhopane (Ts and Tm respectively) and the C_{28} and C_{29} tricyclic terpanes are detectable as very minor components. The saturate fraction and thermodesorption *m/z* 191 traces for this sample correspond closely. The hopane distribution in the Macondo oil's saturate fraction shows a strong predominance of the C_{30} hopane, slightly more Ts than Tm, and a gradual decline in abundance from C_{31} to C_{35} (Figure 9C, Table 3). In Figure 9D, C_{30} hopane predominance is clear, but the other details are poorly registered. As indicated in section 2.2.3, the data shown in Figure 9D were produced by a single heating at 610 °C and indicate that some quality was sacrificed for the advantages provided by a rapid screening procedure.

The Kuwait oil hopanes show a maximum at C_{29}, a low Ts/Tm ratio, and an elevated C_{35}/C_{34} ratio (Figure 9E), all characteristics of petroleums derived from carbonate source rocks (Connan et al., 1986; Peters et al., 2005). The hopane distribution in the thermally-desorbed material is quite similar, but also showing benzohopanes previously noted in the aromatic fraction (Figure 3B). Since thermodesorption was performed on the whole oil sample, saturated and aromatic compounds may both be detected. Aromatic hopanes are also characteristic of carbonate-sourced oils (Connan et al., 1986). The Aboño and *Prestige* fuel oils have similar hopane distributions, with a maximum at C_{30}, relatively abundant C_{29}, Tm, and C_{31}, and a gradual reduction in abundance from C_{31} to C_{35} (Figures 9G, 9I, Table 3). In the Aboño thermodesorption products, the C_{27}, C_{29} and C_{30} proportions resemble those in the saturated fraction (Figures 9G, 9H) but the C_{31}-C_{35} hopanes are poorly resolved, likely due to insufficient concentrations. In contrast, the *Prestige* thermodesorption results compare favorably with

those from the saturated fraction (Figures 9I, 9J). The aromatic C_{33} benzohopane, also detected in the aromatic fraction (Figure 5B), is seen here as a relatively minor component.

<INSERT FIGURE 9 HERE>

Figure 9. Mass chromatograms (*m/z* 191) showing the distribution of hopanes in the saturate fractions (A, C, E, G, I) and corresponding thermodesorption products (B, D, F, H, J) of the five oils. See Table 2 for peak identifications.

The sterane results in Figure 10 are arranged in the same manner as Figures 8 and 9. In the Angola saturated fraction, the regular steranes are relatively more abundant than the rearranged, with C_{29} > C_{27} > C_{28} (Figure 10A). Chromatographic conditions were optimized for biomarker work and near baseline resolution was achieved for individual compounds. Although chromatographic resolution is evidently inferior in the case of the thermodesorption data, the same general picture nonetheless emerges (Figure 10B) in half the analysis time. The Macondo oil is distinguished by a predominance of C_{27} diasteranes (Figure 10C). Although the single temperature, rapid screening experiment poorly resolved the steranes, the importance of the C_{27} diasteranes is clearly evident (Figure 10D). The Kuwait oil has a regular sterane carbon number distribution showing C_{29} > C_{27} > C_{28} with relatively minor diasteranes (Figure 10E), consistent with derivation from carbonate source rock (Connan et al., 1986; Peters et al., 2005). The thermodesorption results provide the same general information, but with poorer chromatographic resolution and signal to noise ratio (Figure 10F).   The Aboño and *Prestige* fuel oils have similar sterane distributions with a modest preference for C_{29} over C_{27} and relatively moderate amounts of C_{28} (Figures 10G, 10I). Rearranged steranes are nearly as abundant as the regular. The

20
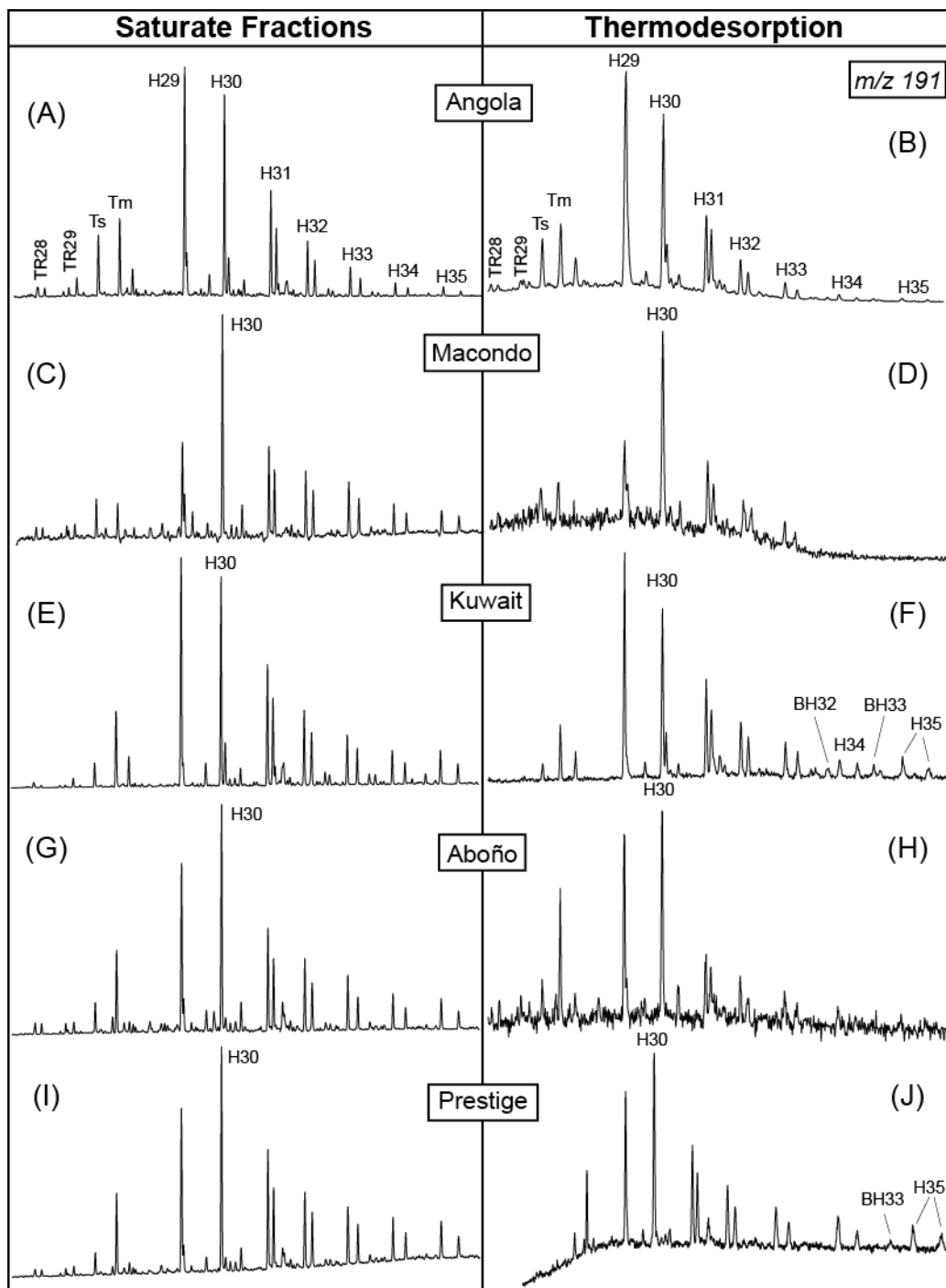
Figure 9

steranes in the Aboño thermodesorption products are poorly discernable with a the low signal to noise ratio (Figure 10H). This would likely have been improved with a larger sample size. Upon thermodesorption, the *Prestige* oil yielded a sterane distribution comparable to that seen in the saturated fraction (Figures 10I, 10J).

<INSERT FIGURE 10 HERE>

Figure 10. Mass chromatograms (*m/z* 71) showing the distribution of steranes in the saturate fractions (A, C, E, G, I) and corresponding thermodesorption products (B, D, F, H, J) of the five oils. See Table 2 for peak identifications.

3.2.3. Polycyclic Aromatic Compounds

3.2.3.1. Phenanthrenes and Dibenzothiophenes in Aromatic Fractions and Thermodesorption Products

As an example, the distribution of phenanthrene and C_1 to C_4-alkylphenanthrenes in the Kuwait oil are displayed on composite mass chromatograms employing the respective molecular ions (Figure 11). In spite of differences in the chromatographic conditions employed (different instruments, GC columns, and GC temperature programs), the results from the aromatic fraction and the thermodesorption of the whole oil exhibit striking similarities. Small variations in the relative retention times of several isomers produced some variation in coelution or separation, as revealed by close comparison of the C_2- and C_3-alkylphenenanthrene fingerprints on both traces (Figures 11A, 11B). The more complex C_4-alkylphenanthrene isomer clusters display the greatest differences. In both cases, the C_2-alkylphenanthrenes are relatively the most abundant.

Figure 10

Saturate Fractions | Thermodesorption

<INSERT FIGURE 11 HERE>
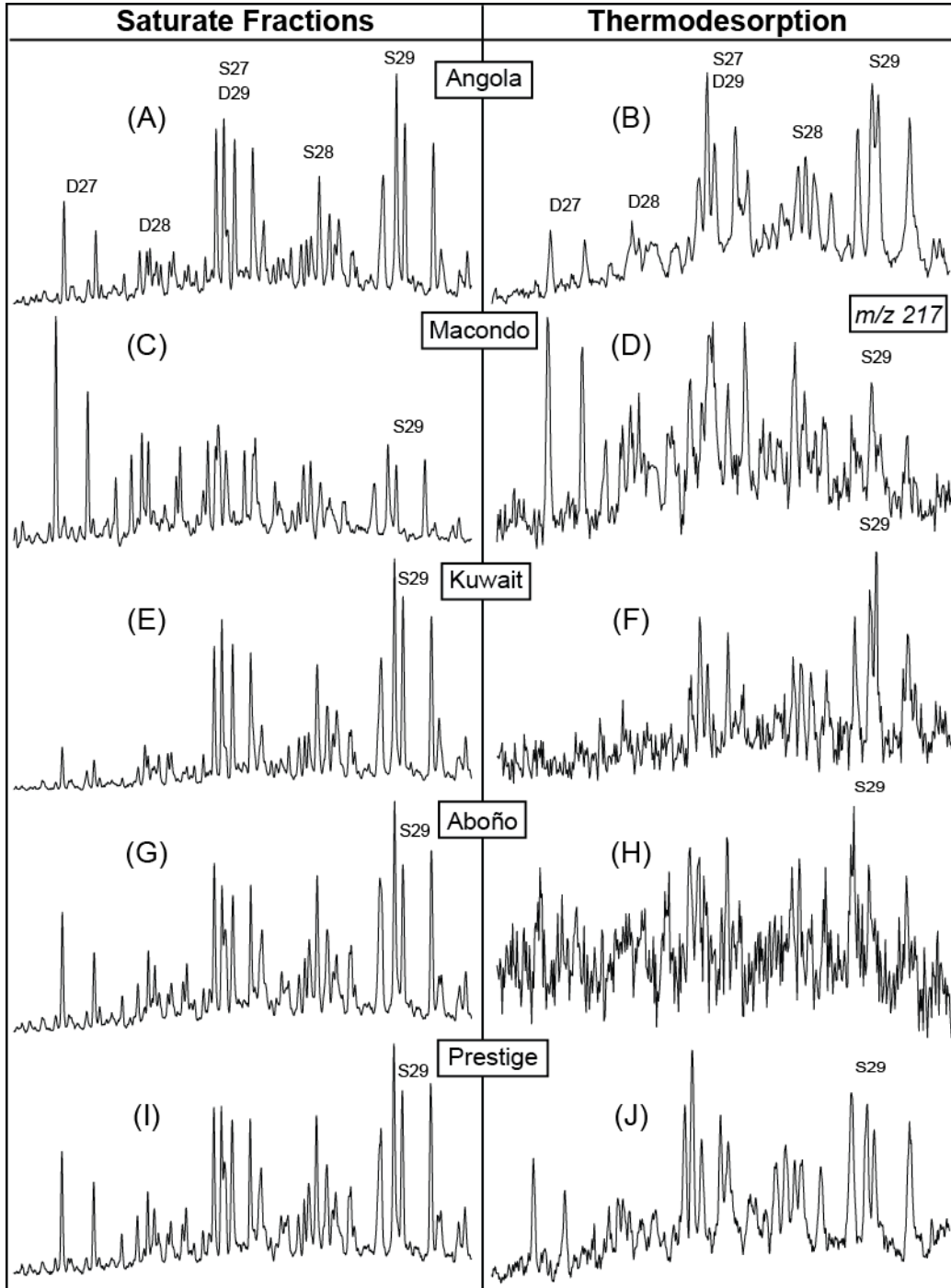
Figure 11. Composite mass chromatograms of the molecular ions of phenanthrene and the C_1 to C_4-alkylphenanthrenes in the A) saturate fraction and B) thermodesorption products of the Kuwait oil. See Table 2 for peak identification.

In analogous fashion, dibenzothiophene and C_1 to C_4-alkyldibenzothiophene fingerprints are shown in Figure 12. The results for the aromatic fraction and thermodesorption closely correspond in overall architecture as well as in detail. As in the phenanthrene example, there are more variations in peak distributions as the degree of alkylation increases. These likely arise due to minor changes in the relative retention times of isomers in response to the differences in the chromatographic conditions. Methylphenanthrene and methyldibenzothiophene ratios show similar trends when calculated for the aromatic fraction and the thermally desorbed products, but exhibit greater variation than that observed with the computed saturated compound ratios (Table 3). Comparisons of PAC ratios based on thermodesorption results with those from solvent extract data should be exercised with caution.

<INSERT FIGURE 12 HERE>

Figure 12. Composite mass chromatograms of the molecular ions of dibenzothiophene and the C_1 to C_4-alkyldibenzothiophenes in the A) saturate fraction and B) thermodesorption products of the Kuwait oil. See Table 2 for peak identification.
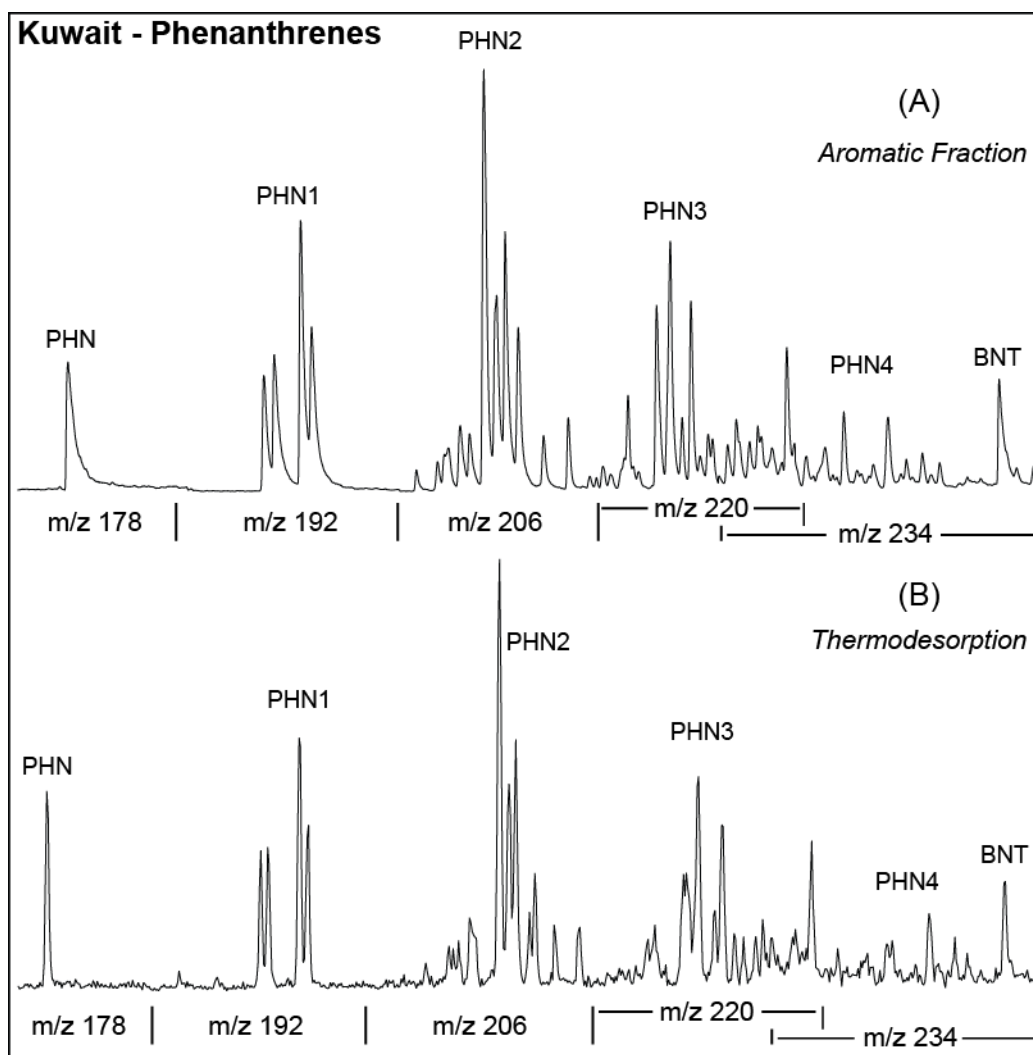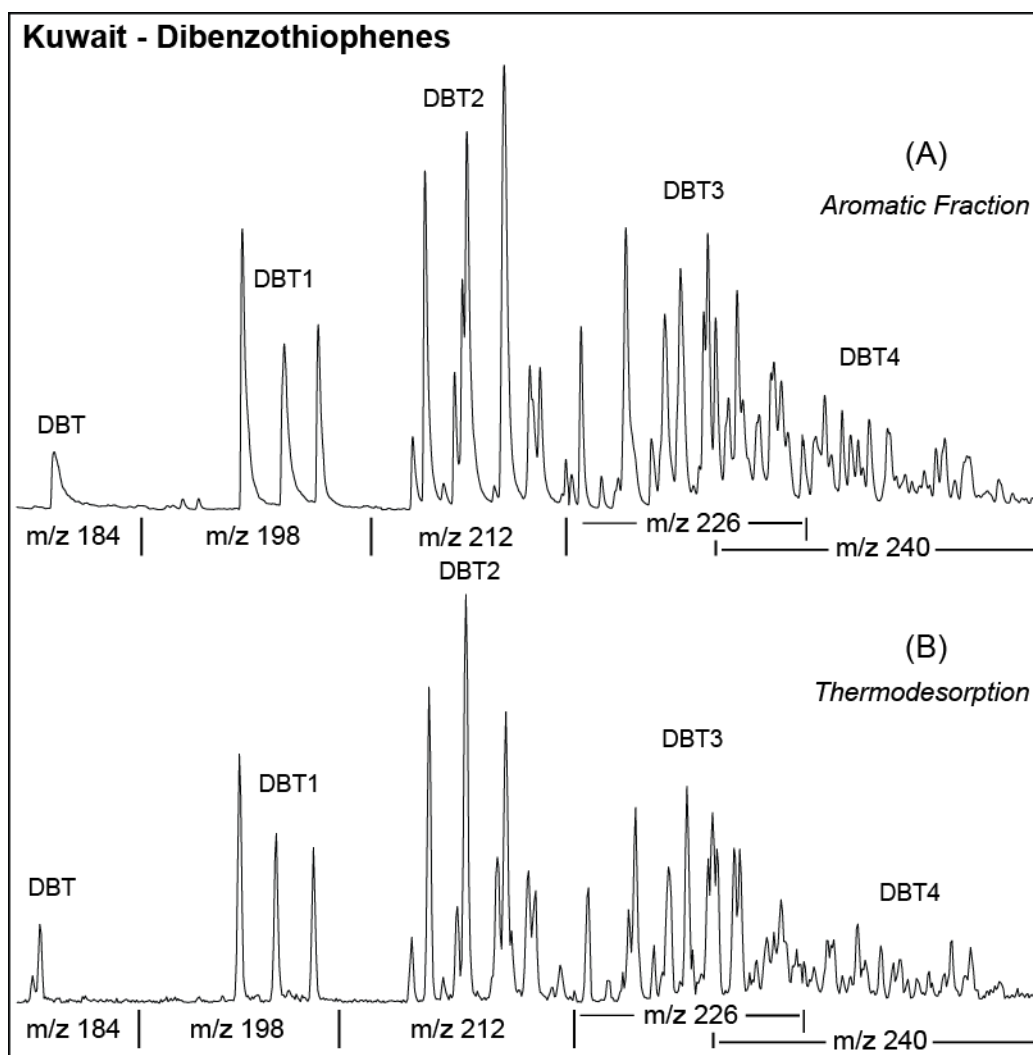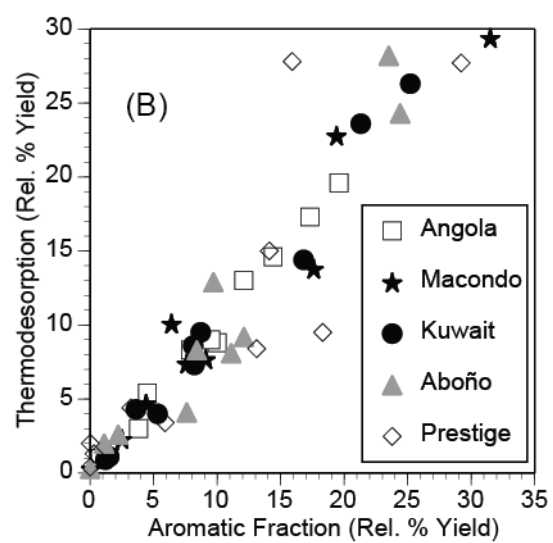
Figure 11

Kuwait - Phenanthrenes

(A)
Aromatic Fraction

PHN2

PHN1

PHN3

PHN

PHN4   BNT

m/z 178 | m/z 192 | m/z 206 | m/z 220 |
m/z 234

(B)
Thermodesorption

PHN2

PHN1

PHN3

PHN

PHN4   BNT

m/z 178 | m/z 192 | m/z 206 | m/z 220 |
m/z 234

Figure 12

Kuwait - Dibenzothiophenes

(A)
Aromatic Fraction

DBT2
DBT3
DBT1
DBT4
DBT

m/z 184   m/z 198   m/z 212   m/z 226   m/z 240

(B)
Thermodesorption

DBT2
DBT3
DBT1
DBT4
DBT

m/z 184   m/z 198   m/z 212   m/z 226   m/z 240

Environmental forensics studies concerned with polycyclic aromatic compounds (PACs) often sum the quantitative results for each isomer cluster (Bence et al., 2007; Stout and Wang, 2007; Wang et al., 2007). For example, the concentrations of all C_2-alkylphenanthrenes are reported as a single composite number, rather than separately presenting the values for the individual constituent isomers. In the case of the phenanthrenes and dibenzothiophenes detected in the Kuwait oil, this can be presented as a simple bar graph, based on the normalized, relative quantitation results employing the relevant molecular ions (Figure 13A). The relatively greater importance of the thiophenic components is clearly evident, consistent with the sample's high sulfur content (Table 1). Among the dibenzothiophenes as well as the phenanthrenes, the C_2- and C_3-alkyl compounds are the most important. Overall the distribution of these compound groups in the aromatic fraction closely resembles that in the thermodesorption products (Fig. 13A). The same holds true for the full set of five samples (Figure 13B), which strongly correlate ($r^2 = 0.89$).

<INSERT FIGURE 13 HERE>

Figure 13. A) Summary bar graphs for the PAC data from Figures 11 and 12 for the aromatic fraction and thermally desorbed products of the Kuwait oil. See Table 2 for compound codes. B) Comparison of the relative PAC yields for the aromatic fractions and thermodesorption products of the five oils. Values for isomer groups have been summed, as in Figure 13A.

3.2.3.2. Polycyclic Aromatic Compounds in Pyrolyzates

Figure 13
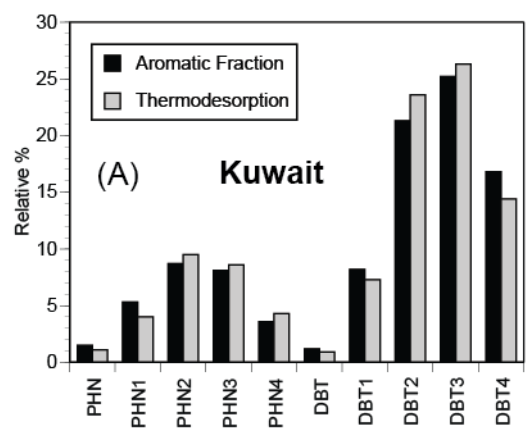
The molecular weight of the pyrolysis products tends to be lower than that of the thermally-desorbed and extracted material, as evident when comparing Figures 3D and 3E with Figures 3A, 3B, and 3C for example. This general observation applies to the occurrence of PACs. These degraded oils have lost their lighter PACs (if they had them originally), but they are produced anew during pyrolysis at 610 °C from the thermodesorption residues and asphaltenes. As an example of this phenomenon, composite mass chromatograms employing molecular ions depict the distributions of naphthalenes and phenanthrenes in the Kuwait oil's pyrolysis products (Figure 14). Among the C_1 to C_3-alkylnaphthalenes, the methylnaphthalenes are relatively the most abundant in both the post-thermodesorption residue and the asphaltene pyrolyzates (Figures 14A, 14B). In overall architecture as well as in the contributions of the individual isomers, the results strongly resemble one another. The samples were analyzed under identical conditions in these experiments, eliminating the instrumental variability discussed in section 3.2.3.1.

<INSERT FIGURE 14 HERE>

Figure 14. Composite mass chromatograms of the molecular ions of C_1 to C_3-alkylnaphthalenes, phenanthrene, and the C_1 to C_2-alkylphenanthrenes in the pyrolysis products of the A) post-thermodesorption residue and B) asphaltenes of the Kuwait oil. See Table 2 for peak identification.

The phenanthrene group fingerprints are also similar in both pyrolyzates, although there is more variation in the proportions of particular isomers (Figures 14C, 14D). The differences between the pyrolysis and thermodesorption products (Figure 11B) are more pronounced. One key difference is the presence of anthracene and its alkylated derivatives in pyrolyzates. The C_3 and C_4-alkylphenanthrenes

Figure 14
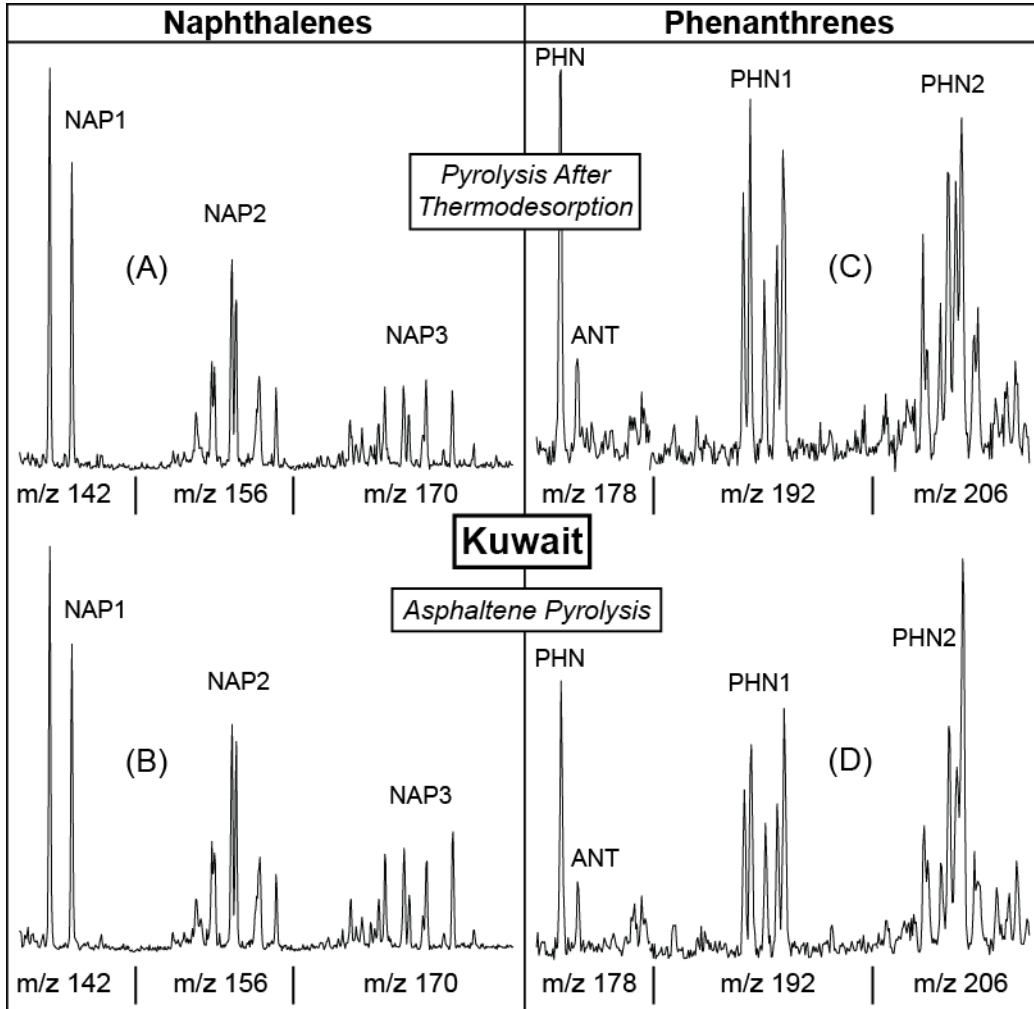
are not well-resolved in the pyrolysis data produced by these samples and are therefore not presented here.

There is a strong resemblance between the alkylbenzothiophene fingerprints of the residue and asphaltene pyrolysis products (Figures 15A, 15B). The 3-ring sulfur compounds in both pyrolyzates are also very similar, overall and in the distribution of individual isomers (Figures 15C, 15D).

<INSERT FIGURE 15 HERE>

Figure 15. Composite mass chromatograms of the molecular ions of C_1 to C_3-benzothiophenes, dibenzothiophene, and the C_1 to C_2-alkyldibenzothiophenes in the pyrolysis products of the A) post-thermodesorption residue and B) asphaltenes of the Kuwait oil. See Table 2 for peak identification.

These observations are summarized graphically using the normalized, relative quantitation results based on the respective molecular ions, summed by PAC compound group (Figure 16A), showing a strong resemblance between the Kuwait residue and asphaltene pyrolyzates. This is also evident for the other samples for which pyrolysis data are available (Figure 16B), which exhibit a robust overall correlation ($r^2 = 0.85$). It can be concluded that the residue pyrolyzed sequentially after thermodesorption is largely comprised of asphaltenes, a conclusion supported by inspection of the pyrolysis TIC traces in Figures 3, 4 and 5. While Angola pyrolyzates (Figures 6D, 6E) appear dominated by contaminants, the PACs are nonetheless revealed on the mass chromatograms of their respective molecular ions, although its asphaltene pyrolysis results are weak and must be interpreted with caution.
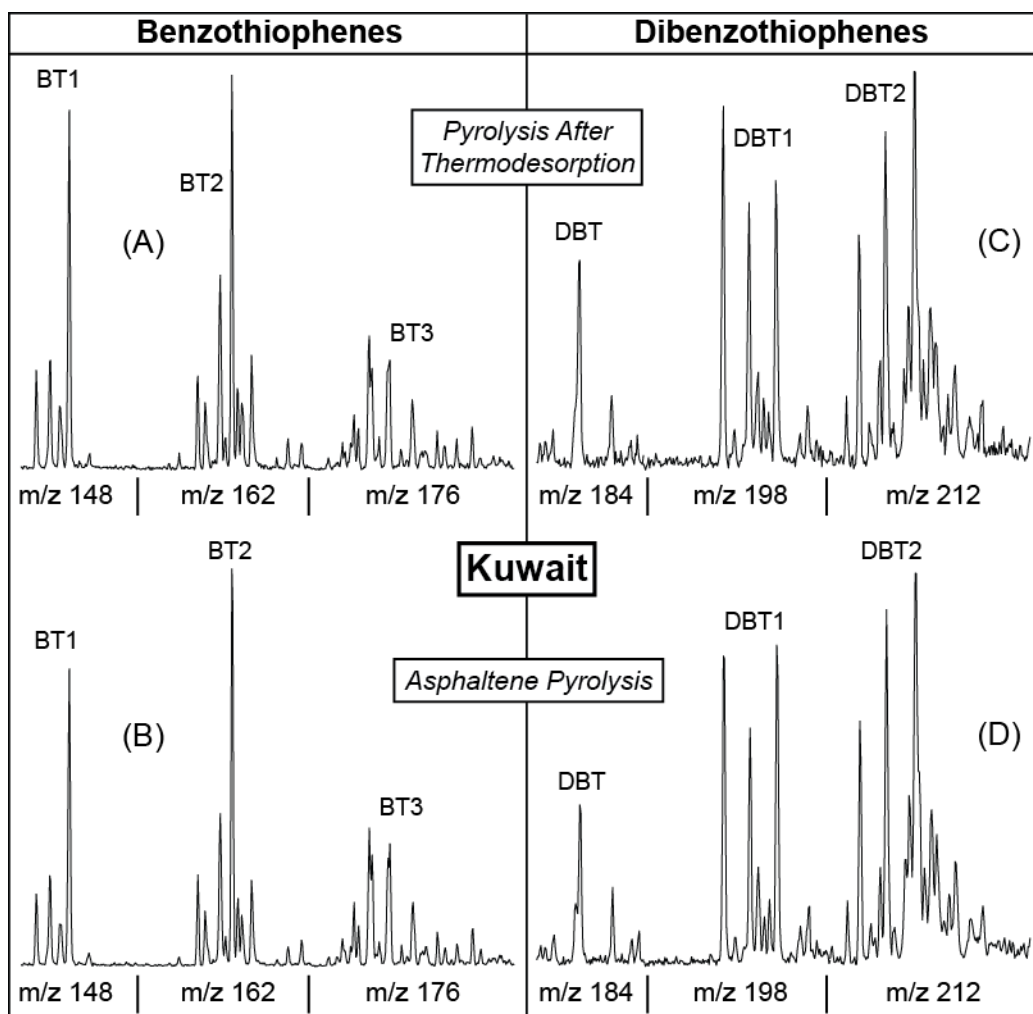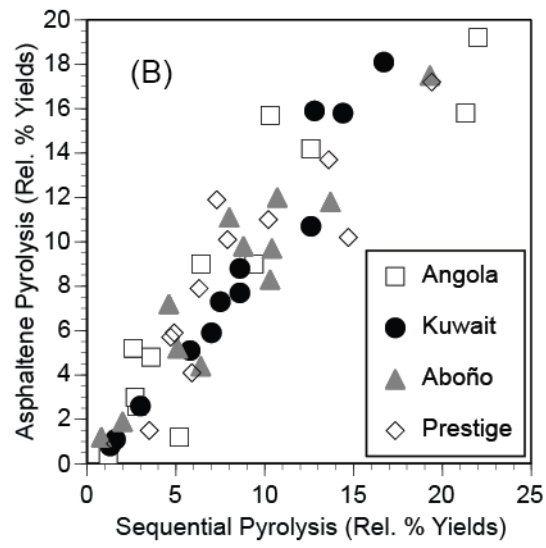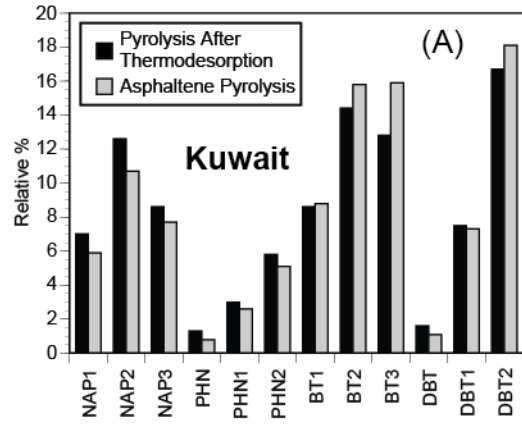
<INSERT FIGURE 16 HERE>

Figure 15

Figure 16

Figure 16. A) Summary bar graphs for the PAC data from Figures 14 and 15 for the pyrolysis products of the post-thermodesorption residue and asphaltenes of the Kuwait oil. See Table 2 for compound codes. B) Comparison of the relative PAC yields for the pyrolysis products of the post-thermodesorption residue and asphaltenes of the four oils for which data are available. Values for isomer groups have been summed, as in Figure 16A.

It is evident that thiophenic compounds are particularly important in the sulfur-rich Kuwait oil sample (Figures 3B, 13A, 16A). This observation is generalized using the Benzothiophene Naphthalene Ratio, defined for pyrolyzates as:

*C₁ to C₃-alkylbenzothiophenes/(C₁ to C₃-alkylnaphthalenes + C₁ to C₃-alkylbenzothiophenes)*

This ratio increases linearly as a function of sulfur content. Notably, the asphaltene pyrolyzates consistently exhibit slightly higher values than those from the corresponding residues (Figure 17).

<INSERT FIGURE 17 HERE>

Figure 17. Cross-plot of total oil sulfur vs. the Benzothiophene Naphthalene Ratio values computed for the pyrolysis products of the post-thermodesorption residue and asphaltenes of the four oils for which data are available. The ratio is computed as [C_1 to C_3-alkylbenzothiophenes/(C_1 to C_3-alkylnaphthalenes + C_1 to C_3-alkylbenzothiophenes)] employing the respective molecular ions (m/z 142, 148, 156, 162, 170, 178).

3.2.4. Alkanones

Figure 17
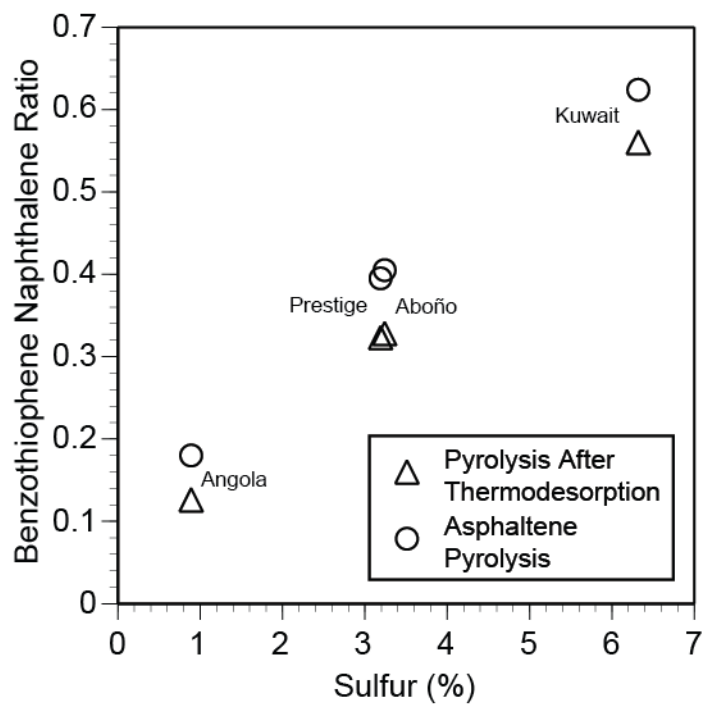
The polar fractions of the five samples were analyzed by GC-MS without prior derivatization (derivatization being beyond the scope of the project). The non-derivatized Aboño, Kuwait and *Prestige* samples revealed little beyond phthalates likely introduced during sample handling and UCM. However, the Angola and Macondo samples contained series of long-chain alkanone isomer groups, C_{14} to C_{27} for the Angola oil and C_{17} to C_{33} for the Macondo, crowning broad UCM humps (Figure 18). Each cluster contains a similar group of peaks, for which the C_{20} provides a representative example (Figure 19), distinguishable here due to the high-resolution gas chromatographic conditions employed. Isomer assignments can be made on the basis of the mass spectra and elution patterns, by reference to the work of Leif and Simoneit (1995) that employed authentic standards. The carbonyl oxygen can attach to the straight hydrocarbon chain at any position. Thus in the case of C_{20}, there is eicosan-2-one, eicosane-3-one, etc., up to at least eicosan-7-one (Figure 19). The 7-one peak is large and likely includes as coeluants the remaining possible isomers up to the 10-one, which is the limit for the C_{20} alkanone.

<INSERT FIGURE 18 HERE>

Figure 18. Total ion current traces of the polar fractions of the A) Angola oil and B) Macondo oil samples. The elution region of the C_{20} alkanones is highlighted.

<INSERT FIGURE 19 HERE>

Figure 19. Details of the C_{20} alkanones detected in the Macondo (A-E) and Angola (F-J) oil samples, employing the total ion current and the m/z 57, 58, 71, and 72 traces. Peaks are labeled according to the position of the carbonyl function (-2-: eicosan-2-one, -3-: eicosan-3-one, etc.); *n*-C_{22} is *n*-docosane.

Figure 18

(A)
Angola

C_{20} alkanones

(B)
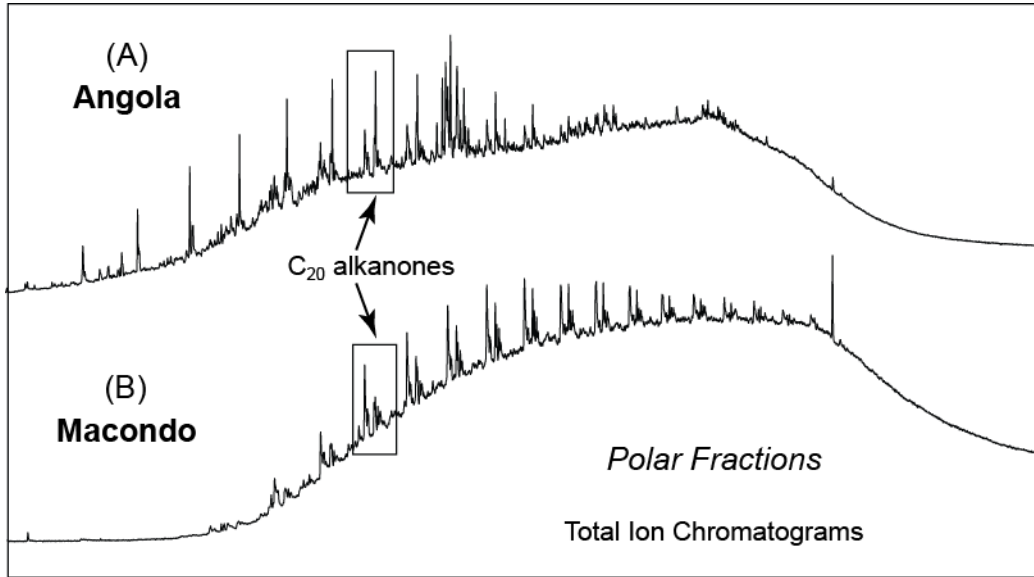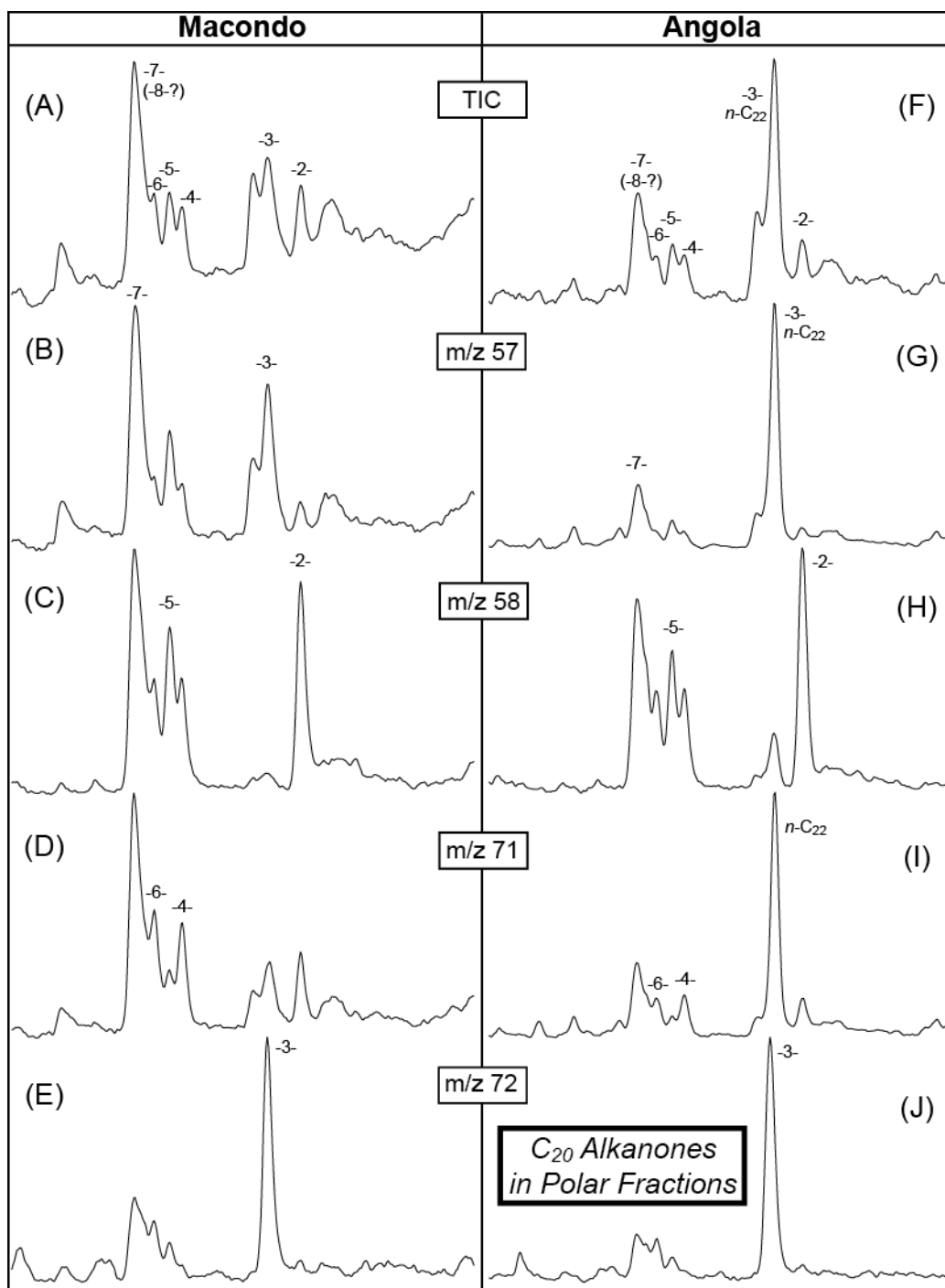**Macondo**

Polar Fractions

Total Ion Chromatograms

Figure 19

The eicosanone isomers in the Macondo oil are readily discernable on the total ion current trace (Figure 19A). Eicosan-3-one and 7-one are emphasized on the m/z 57 trace, while the 2-one and 5-one appear stronger on the m/z 58 (Figures 19B, 19C). The 4-one and 6-one are best observed on the m/z 71 mass chromatogram and m/z 72 highlights eicosan-3-one (Figures 19D, 19E). The same pattern is observed in the Angola oil's polar fraction, but with the addition of the C_{22} n-alkane coeluting with the eicosan-3-one (Figures 19F-19J). This oil is so enriched in saturated hydrocarbons (71.6 %, Table 1), that the liquid chromatographic system was evidently overwhelmed and some normal alkanes eluted with the polar fraction. Alkanones were not detected in the thermodesorption and pyrolysis products.

Oxygen-containing compounds occur in significant variety and abundance in weathered Macondo oil, evidently as products of post-spill alteration (Aeppli et al., 2012; Ruddy et al., 2014; Chen et al., 2016; White et al., 2016), with alkan-2-ones among them (Ruddy et al., 2014). In the present study, additional alkanone isomers are identified in Macondo oil, as well as in the Angola sample. However, the alkanones were not detected in the Kuwait, Aboño, and *Prestige* oils. While all five oils are weathered, a key distinction is that the Angola and Macondo samples are particularly enriched in saturated hydrocarbons but the others are not (Table 1). It would appear that aliphatic-rich oils are the most prone to formation of ketones upon weathering.

The Macondo and Angola oils are also the ones containing long-chain alkylbenzenes in their aromatic fractions (Figures 6B, 7B), compounds that have been previously noted in aliphatic-rich source rock and petroleum (Ellis et al., 1996; Zhang et al., 2014). In contrast to the ketones, these compounds are likely primary components rather than weathering products. Together with the normal alkanes and ketones, the alkylbenzenes reflect the aliphatic nature of the oils.

4. Conclusions

A multi-faceted environmental forensics approach revealed key molecular features of a diverse, genetically-unrelated suite of weathered spilled oils. In addition to the commonly employed GC/MS analysis of saturated and aromatic fractions, the polar fractions were investigated. These experiments led to the recognition of a complex series of linear alkanones in those oil samples particularly enriched in aliphatics. Thermodesorption-GC-MS of the whole oils was used to further test its efficacy as a tool for the rapid fingerprinting of environmental contamination. The method was shown to accurately detect most of the essential features recognized in the conventional analysis of the saturated and aromatic fractions, although in some instances with less sensitivity and poorer resolution. Characteristics so recognized included the distributions of normal and isoprenoid alkanes, saturate and aromatic biomarkers, and polycyclic aromatic compounds such as alkylphenanthrenes and alkyldibenzothiophenes.

Sequential pyrolysis of the post-thermodesorption residue and asphaltene pyrolysis yielded similar results, indicating that the residue is likely to consist primarily of asphaltenes. A ratio of pyrolytic benzothiophenes to naphthalenes correlates with the sulfur content of the oils. Thermodesorption and pyrolysis also recognized substances likely to be associated with spill cleanup efforts that were not detected by conventional analysis.

References

Abdullah, F.H. and J. Connan. Geochemical study of some Cretaceous rocks from Kuwait: comparison with oils from Cretaceous and Jurassic reservoirs. Organic Geochemistry; 2002; 33, 125-148.

Aeppli, C., C.A. Carmichael, R.K. Nelson, K.L. Lemkau, W.M. Graham, M.C. Redmond, D.L. Valentine and C.M. Reddy. Oil weathering after the Deepwater Horizon disaster Led to the formation of oxygenated residues. Environmental Science & Technology; 2012; 46, 8799-8807.

Aeppli, C., R.K. Nelson, J.R. Radović, C.A. Carmichael, D.L. Valentine and C.M. Reddy. Recalcitrance and degradation of petroleum biomarkers upon abiotic and biotic natural weathering of Deepwater Horizon oil. Environmental Science & Technology; 2014; 48, 6726-6734.

Alzaga, R., P. Montuori, L. Ortiz, J.M. Bayona and J. Albaigés. Fast solid-phase extraction–gas chromatography–mass spectrometry procedure for oil fingerprinting: Application to the *Prestige* oil spill. Journal of Chromatography A; 2004; 1025, 133-138.

Atlas, R.M. and T.C. Hazen. Oil biodegradation and bioremediation: A tale of the two worst spills in U.S. history. Environmental Science & Technology; 2011; 45, 6709-6715.

Balba, M.T., R. Al-Daher, N. Al-Awadhi, H. Chino and H. Tsuji. Bioremediation of oil-contaminated desert soil: The Kuwaiti experience. Environment International; 1998; 24, 163-173.

Bence, A.E., D.S. Page and P.D. Boehm. Advances in forensic techniques for petroleum hydrocarbons: The Exxon Valdez experience; In: Z. Wang, S.A. Stout Eds.; Oil Spill Environmental Forensics; Academic Press, Burlington (MA); 2007; 449-487.

Brown, L.D., D.L. Cologgi, K.F. Gee and A.C. Ulrich. Bioremediation of oil spills on land; In: M. Fingas Ed.; Oil Spill Science and Technology; Gulf Professional Publishing, Boston; 1998; 699-729.

Chen, H., A. Hou, Y.E. Corilo, Q. Lin, J. Lu, I.A. Mendelssohn, R. Zhang, R.P. Rodgers and A.M. McKenna. 4 Years after the Deepwater Horizon spill: Molecular transformation of Macondo well oil in Louisiana salt marsh sediments revealed by FT-ICR mass spectrometry. Environmental Science & Technology; 2016; 50, 9061-9069.

Connan, J., J. Bouroullec, D. Dessort and P. Albrecht. The microbial input in carbonate-anhydrite facies of a sabkha palaeoenvironment from Guatemala: A molecular approach. Organic Geochemistry; 1986; 10, 29-50.

De Leeuw, J.W., E.W.B. De Leer, J.S.S. Damste and P.J.W. Schuyl. Screening of anthropogenic compounds in polluted sediments and soils by flash evaporation/pyrolysis gas chromatography-mass spectrometry. Analytical Chemistry; 1986; 58, 1852-1857.

Díez, S., J. Sabaté, M. Viñas, J.M. Bayona, A.M. Solanas and J. Albaigés. The *Prestige* oil spill. I. Biodegradation of a heavy fuel oil under simulated conditions. Environmental Toxicology and Chemistry; 2005; 24, 2203-2217.

Ellis, L., T.A. Langworthy and R. Winans. Occurrence of phenylalkanes in some Australian crude oils and sediments. Organic Geochemistry; 1996; 24, 57-69.

Faure, P. and P. Landais. Rapid contamination screening of river sediments by flash pyrolysis-gas chromatography–mass spectrometry (PyGC–MS) and thermodesorption GC–MS (TdGC–MS). Journal of Analytical and Applied Pyrolysis; 2001; 57, 187-202.

Gaines, R.B., G.S. Frysinger, C.M. Reddy and R.K. Nelson. Oil spill source identification by comprehensive two-dimensional gas chromatography (GCXGC); In: Z. Wang, S.A. Stout Eds.; Oil Spill Environmental Forensics; Academic Press, Burlington (MA); 2007; 169-206.

Gallego, J.R., J.R. Fernández, F. Díez-Sanz, S. Ordoñez, H. Sastre, E. González-Rojas, A.I. Peláez and J. Sánchez. Bioremediation for shoreline cleanup: In situ vs. on-site treatments. Environmental Engineering Science; 2007; 24, 493-504.

Gallego, J.R., E. González-Rojas, A.I. Peláez, J. Sánchez, M.J. García-Martínez, J.E. Ortiz, T. Torres and J.F. Llamas. Natural attenuation and bioremediation of *Prestige* fuel oil along the Atlantic coast of Galicia (Spain). Organic Geochemistry; 2006; 37, 1869-1884.

Gallego, J.R., A. Lara-Gonzalo, E. Rodríguez-Valdés, G. Márquez and M. Escobar. Natural attenuation of heavy fuel oil components along oiled shores. 26th International Meeting on Organic Geochemistry; Tenerife (Spain); 2013.

Jeffrey, A.W.A. Application of stable isotope ratios in spilled oil identification; In: Z. Wang, S.A. Stout Eds.; Oil Spill Environmental Forensics; Academic Press, Burlington (MA); 2007; 207-227.

Kaufman, R.L., C.S. Kabir, B. Abdul-Rahman, R. Quttainah, H. Dashti, J.M. Pederson and M.S. Moon. Characterizing the Greater Burgan field with geochemical and other field data. SPE Reservoir Evaluation & Engineering; 2000; 3, 118-126.

Kruge, M.A. Analytical pyrolysis principles and applications to environmental science; In: M. Barbooti Ed.; Environmental Applications of Instrumental Chemical Analysis; CRC Press, Boca Raton (FL); 2015; 533-569.

Kruge, M.A. and A. Permanyer. Application of pyrolysis-GC/MS for rapid assessment of organic contamination in sediments from Barcelona harbor. Organic Geochemistry; 2004; 35, 1395-1408.

Kruge, M.A., A. Permanyer, J. Serra and D. Yu. Geochemical investigation of an offshore sewage sludge deposit, Barcelona, Catalonia, Spain. Journal of Analytical and Applied Pyrolysis; 2010; 89, 204-217.

Lara-Gonzalo, A., M.A. Kruge, I. Lores, B. Gutiérrez and J.R. Gallego. Pyrolysis GC–MS for the rapid environmental forensic screening of contaminated brownfield soil. Organic Geochemistry; 2015; 87, 9-20.

Leif, R.N. and B.R.T. Simoneit. Ketones in hydrothermal petroleums and sediment extracts from Guaymas Basin, Gulf of California. Organic Geochemistry; 1995; 23, 889-904.

Peters, K.E., C.C. Walters and J.M. Moldowan. The Biomarker Guide. Vol. 2. Biomarkers and Isotopes in Petroleum Exploration and Earth History; Cambridge University Press; Cambridge; 2005; 1155 p.

Reddy, C.M., J.S. Arey, J.S. Seewald, S.P. Sylva, K.L. Lemkau, R.K. Nelson, C.A. Carmichael, C.P. McIntyre, J. Fenwick, G.T. Ventura, B.A.S. Van Mooy and R. Camilli. Composition and fate of gas and oil released to the water column during the Deepwater Horizon oil spill. Proceedings of the National Academy of Sciences; 2012; 109, 20229-20234.

Richnow, H.H., R. Seifert, M. Kästner, B. Mahro, B. Horsfield, U. Tiedgen, S. Böhm and W. Michaelis. Rapid screening of PAH-residues in bioremediated soils. Chemosphere; 1995; 31, 3991-3999.

Ruddy, B.M., M. Huettel, J.E. Kostka, V.V. Lobodin, B.J. Bythell, A.M. McKenna, C. Aeppli, C.M. Reddy, R.K. Nelson, A.G. Marshall and R.P. Rodgers. Targeted petroleomics: Analytical investigation of Macondo well oil oxidation products from Pensacola Beach. Energy & Fuels; 2014; 28, 4043-4050.

Stout, S.A. and Z. Wang. Chemical fingerprinting of spilled or discharged petroleum — methods and factors affecting petroleum fingerprints in the environment; In: Z. Wang, S.A. Stout Eds.; Oil Spill Environmental Forensics; Academic Press, Burlington (MA); 2007; 1-53.

Tissot, B.P. and D.H. Welte. Petroleum Formation and Occurrence; Springer; 1984; 702 p.

USEPA. Semivolatile organic compounds (PAHs and PCBs) in soils/sludges and solid wastes using thermal extraction/gas chromatography/mass spectrometry (TE/GC/MS). EPA Method 8275A.; U.S. Environmental Protection Agency; Washington, D.C.; 1996; 1-23 p.

Vollhardt, K.P.C. and N.E. Schore. Organic Chemistry: Structure and Function; W. H. Freeman; New York; 2002; 1203 p.

Wang, Z., C. Yang, M. Fingas, B. Hollebone, U. Hyuk Yim and J. Ryoung Oh. Petroleum biomarker fingerprinting for oil spill characterization and source identification; In: Z. Wang, S.A. Stout Eds.; Oil Spill Environmental Forensics; Academic Press, Burlington (MA); 2007; 73-146.

Whelan, J.K., J.M. Hunt and A.Y. Huc. Applications of thermal distillation—pyrolysis to petroleum source rock studies and marine pollution. Journal of Analytical and Applied Pyrolysis; 1980; 2, 79-96.

White, H.K., C.H. Wang, P.L. Williams, D.M. Findley, A.M. Thurston, R.L. Simister, C. Aeppli, R.K. Nelson and C.M. Reddy. Long-term weathering and continued oxidation of oil residues from the Deepwater Horizon spill. Marine Pollution Bulletin; 2016; 113, 380-386.

Zhang, S., H. Huang, J. Su, M. Liu and H. Zhang. Geochemistry of alkylbenzenes in the Paleozoic oils from the Tarim Basin, NW China. Organic Geochemistry; 2014; 77, 126-139.